

TGOSPA Metric Parameters Selection and Evaluation for Visual Multi-object Tracking

Jan Krejčí

University of West Bohemia, Pilsen, Czech Republic

Oliver Kost

University of West Bohemia, Pilsen, Czech Republic

Ondřej Straka, Member, IEEE

University of West Bohemia, Pilsen, Czech Republic

Yuxuan Xia

Shanghai Jiaotong University, Shanghai, China

Lennart Svensson, Senior Member, IEEE

Chalmers University of Technology, Göteborg, Sweden

Ángel F. García-Fernández

University of Liverpool, Liverpool, United Kingdom

Abstract— Multi-object tracking algorithms are deployed in various applications, each with unique performance requirements. For example, track switches pose significant challenges for offline scene understanding, as they hinder the accuracy of data interpretation. Conversely, in online surveillance applications, their impact is often minimal. This disparity underscores the need for application-specific performance evaluations that are both simple and mathematically sound. The trajectory generalized optimal sub-pattern assignment (TGOSPA) metric offers a principled approach to evaluate multi-object tracking performance. It accounts for localization errors, the number of missed and false objects, and the number of track switches, providing a comprehensive assessment framework. This paper illustrates the effective use of the TGOSPA metric in computer vision tasks, addressing challenges posed by the need for application-specific scoring methodologies. By exploring the TGOSPA parameter selection, we enable users to compare, comprehend, and optimize the performance of algorithms tailored

Manuscript received XXXXX 00, 0000; revised XXXXX 00, 0000; accepted XXXXX 00, 0000.

The work was supported by the Ministry of Education, Youth and Sports of the Czech Republic under project ROBOPROX - Robotics and Advanced Industrial Production CZ.02.01.01/00/22_008/0004590. (Corresponding author: J. Krejčí)

Author's addresses: Jan Krejčí, Oliver Kost and Ondřej Straka are with the Department of Cybernetics, University of West Bohemia, Pilsen, Czech Republic (e-mail: {jcrejci, kost, straka30}@kky.zcu.cz). Yuxuan Xia is with Department of Automation, Shanghai Jiaotong University, Shanghai, China (e-mail: yuxuan.xia@sjtu.edu.cn). Lennart Svensson is with Signal Processing Group, Chalmers University of Technology, Göteborg, Sweden (e-mail: lennart.svensson@chalmers.se). Ángel F. García-Fernández is with Department of Electrical Engineering and Electronics, University of Liverpool, Liverpool, United Kingdom (e-mail: angel.garcia-fernandez@liverpool.ac.uk)

0018-9251 © 2025 IEEE

for specific tasks, such as target tracking and training of detector or re-ID modules.

Index Terms— Performance evaluation, multiple object tracking, sets of trajectories, visual tracking.

I. Introduction

ESTIMATING the number and locations of objects appearing in a given surveillance area is addressed by algorithms for object detection and tracking [1]–[4]. Their development and implementation have significant potential in various fields, including aerial and naval security [1], medical applications [5], and space situational awareness [6], among others. This paper mainly focuses on applications that utilize computer vision (CV), though most results presented are generally applicable. In particular, this paper considers the case when a single monocular camera is used to perform detection/tracking with objects represented by two-dimensional bounding boxes. Such applications are essential for public safety monitoring, autonomous driving, and many others.

Evaluating the detection and tracking algorithms is key for their convenient selection for particular applications and, thus, their development. The selection should, however, consider application-specific needs that usually differ among applications. While there are many aspects one could consider when evaluating algorithm performance [7], such as estimation consistency, computational demands, or numerical stability, this paper focuses solely on the evaluation based on empirical data. Algorithm results, specifically point estimates (mere bounding boxes), must be obtained for applications where ground truth data, also known as annotations, are available. The results of the algorithm and the ground truth data are then *compared* to each other using a performance evaluation function that yields a single *value*. To be able to reason among multiple algorithms based on the corresponding evaluation results, the evaluation should capture the efficiency of the algorithms. In particular, the evaluation should be able to differentiate between algorithms producing different results and clearly justify the difference.

In the CV field, the performance evaluation is usually based on computing *scores*, further called CV scores. The Multiple object tracking accuracy (MOTA), Higher order tracking accuracy (HOTA), and Identity F1 (IDF1) scores are often considered authoritative in CV literature [8]–[11]. They are also listed as the first three scores in the MOT17 benchmark website [12]. In particular, HOTA was shown to solve several known problems encountered in the other CV scores [10]. Although the scores are commonly referred to as *metrics* in the CV community, the scores generally fail to fulfill the mathematical properties required for a function to be a metric. That is, the identity, symmetry, and triangle inequality properties [13]. The only CV score that is presented in the literature as a mathematical metric is the *Higher-order tracking accuracy* (HOTA) [10]. This paper reveals that HOTA still

may have undesirable behavior, and moreover, it shows that HOTA is not a metric in the mathematical sense.

To address the inconvenience, this paper proposes to use the *Trajectory generalized optimal sub-pattern assignment* (TGOSPA) metric [14], [15]. Similarly to the CV scores, TGOSPA assigns ground truth objects to estimates at each time step and penalizes (i) the distance between pairs of assigned objects and estimates, (ii) the number of missed objects, (iii) number of false estimates, and (iv) the number of track switches¹. Although most CV scores capture some of TGOSPA properties, their definitions are rather heuristic [10]. TGOSPA, on the other hand, penalizes all these different quantities in a principled mathematical manner by being a metric [14], [15].

Different applications may allow, e.g., different distance errors or different tolerances for track switches. TGOSPA introduces (hyper-)parameters that can reflect various user preferences to *tailor* the evaluation to an application at hand. The parameters include (I) a *cut-off* parameter setting the maximum possible distance between ground truth and an estimate, (II) an *exponent* parameter that penalizes outliers, and (III) a *switching penalty* that penalizes track switches. The parameters must be selected before the evaluation. In the literature, however, the effects of the parameter selection are rarely discussed, except for their general interpretation.

Note that there is several alternatives to TGOSPA in the literature [16]–[19]. In particular, the favorable properties of TGOSPA compared to the *Bento's* metrics [16] are analyzed in [14]. The version of *Optimal sub-pattern assignment metric* (OSPA) called OSPA⁽²⁾ [17] does not penalize all quantities (i)–(iv) mentioned above. The same is true for the OSPA for tracks (OSPAT) [18], which is, moreover, not a metric and was analyzed in [19]. In addition, the OSPA for multiple tracks (OSPAMT) was introduced in [19], which is, however, computationally intractable for most practical problems [17] and does not have a clear interpretation in terms of quantities (i)–(iv).

In this paper, we introduce TGOSPA as a principled metric for CV multi-object tracking evaluation and provide guidelines for selecting its parameters. The key contributions of the paper are as follows:

- The TGOSPA metric is introduced in the context of CV.
- The effects of TGOSPA parameters are revealed in general, including their graphical interpretation.
- A *method* for the TGOSPA parameters selection is proposed and exemplified for CV.
- Evaluation examples illustrate the impact of the different TGOSPA parameters, facilitating easier parameter selection in practice.
- It is shown that the HOTA score is not a metric.
- Illustrative examples highlight the differences between TGOSPA and HOTA.

¹In the CV community, the term *identity* switch is used more often.

The outline of the paper is summarized as follows. Section II introduces a visual tracking example and Section III motivates the need for a convenient performance evaluation metric. The TGOSPA metric is then introduced in Section IV, together with the general explanation of its parameter effects. Application-dependent selection of the parameters is then discussed in Section V and performance evaluation examples are given in Section VI. TGOSPA is then compared to HOTA in Section VII and the paper concludes in Section VIII.

II. Studied Scenario and Applied Algorithms

This section presents the scenario and algorithms that will be used to analyze the performance measures.

A. Scenario

Consider the MOT17-09 video from the MOT17 dataset [9] available online at [12]. Between time steps $k_0=382$ and $k_F=442$ in that video (61 frames, 2 seconds²), two pedestrians being annotated with the ground truth IDs 2 and 6, denoted as *gt2* and *gt6*, respectively, cross each other. This leads to a challenging occlusion scenario depicted in Fig. 1. In this paper, five selected algorithms are to be evaluated in this scenario using several different performance scores. Note that only the two-dimensional bounding boxes in the image frame are considered in the evaluation. The algorithms and a short description of their corresponding tracking results follow.

B. Algorithms

FRCNN detector: The Faster R-CNN (FRCNN) [20] detector, whose outputs are included in the MOT17 dataset, processes each frame individually. Consequently, the results from the FRCNN detector are not temporally connected in time and do not form trajectories. As illustrated in Fig. 2, the detections match the ground truth bounding boxes seemingly well. However, detections are missing for the occluded pedestrian between time steps 409 and 421, i.e., for 13 time steps.

Tracktor++v2 tracker: The Tracktor++v2 introduced in [21] is evaluated using the MOT17 benchmark, where it processes the FRCNN detections and produces trajectories. As illustrated in Fig. 3, the occluded pedestrian is not tracked between time steps 412 and 420, i.e., for 9 time steps. In particular, two different trajectories are produced for the occluded pedestrian *gt6*; the first, marked with ID 25, is present before the occlusion, while the second, marked with ID 28, appears after the occlusion. This situation is called *track fragmentation*. In general, such behavior is referred to as *long-term track change* in this paper. In performance evaluation, a score should be capable of classifying such events as a *switch*.

²The frame rate for the MOT17-09 video is 30 fps.



Fig. 1: Part of the publicly available MOT17-09 scenario studied in this paper. The ground truth objects are depicted in blue. The blue traces depict past locations of the bottom-center point.

BoT_SORT tracker: Bag-of-tricks for simple online and real-time tracking (Bot_SORT) based method [22] processes custom detections based on a pre-trained YOLOX detector [23]. The used version of BoT_SORT employs linear interpolation and is effectively an offline method. As depicted in Fig. 4, both objects are tracked during the entire scenario, except for a single peculiarity appearing during the occlusion at time step 415. At that single time step, the two estimated tracks seemingly switch positions as if they swapped the ground truth object they were tracking before and after that time step. That is, several switches seemingly occur for a single time step and it might be caused by an error of the re-ID module combined with linear interpolation employed in the tracker. Such behavior is referred to as a *short-term interim track change* in this paper. From Fig. 4c, notice that a considerable misalignment of the estimated bounding boxes w.r.t. the ground truth bounding boxes appear at time step $k=416$.

GMPHDOGMI7 tracker: The online tracker introduced in [24] is based on the Gaussian mixture probability hypothesis density (GM-PHD) filter and employs the occlusion group energy minimization (OGEM). The tracker processes FRCNN detections and is an online method. As illustrated in Fig. 5, all pedestrians are tracked. During the occlusion of the pedestrian *gt6*, however, the tracker outputs only predictive estimates (with ID 41). The predictive boxes may exceed a certain level of error further called as *maximum admissible error* defined by the user for certain applications, e.g., starting at the time step $k=403$ (see Fig. 5a) until *better* estimates are produced again at time step 422.

Note that results generated from the above algorithms, except³ for BoT_SORT, were downloaded directly from the MOT17 website [12]. To analyze the particular MOT17-09 occlusion scenario (Fig. 1), both the ground truth and estimation results were processed by hand to include only the data corresponding to the ground truth IDs 2 and 6 between $k_0=281$ and $k_F=442$.

³Results from the BoT_SORT algorithm were generated by using the publicly available code at github.com/NirAharon/BoT-SORT/.

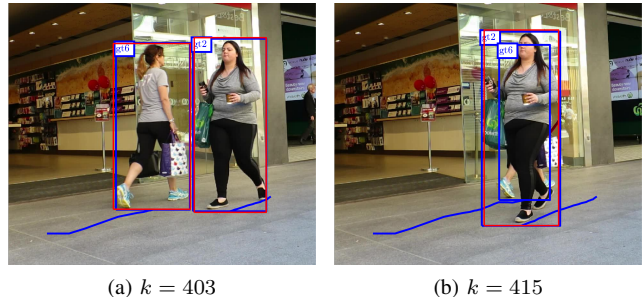


Fig. 2: FRCNN detector results depicted in red. The detector processes each frame individually, and the estimates are thus not connected over time.



Fig. 3: Tractor++v2 tracker results. The pedestrian *gt6* is not tracked when it is occluded, and a new track is initiated afterward.

III. Motivation

This section motivates the necessity for a performance evaluation score with superior properties compared to those currently used in the CV community. The need is demonstrated through a tracking scenario indicating that the CV scores do not meet various requirements.

Using the data corresponding to the scenario from Section II, the MOTA, HOTA, and IDF1 scores for the

TABLE I: Algorithms results evaluated using commonly used scores. The higher the value, the better.

	MOTA (\uparrow)	IDF1 (\uparrow)	HOTA (\uparrow)
FRCNN detector	0.016	0.017	0.119
Tractor++v2 tracker	0.918	0.774	0.789
BoT_SORT tracker	1	1	0.921
GMPHDOGMI7 tracker	1	1	0.942

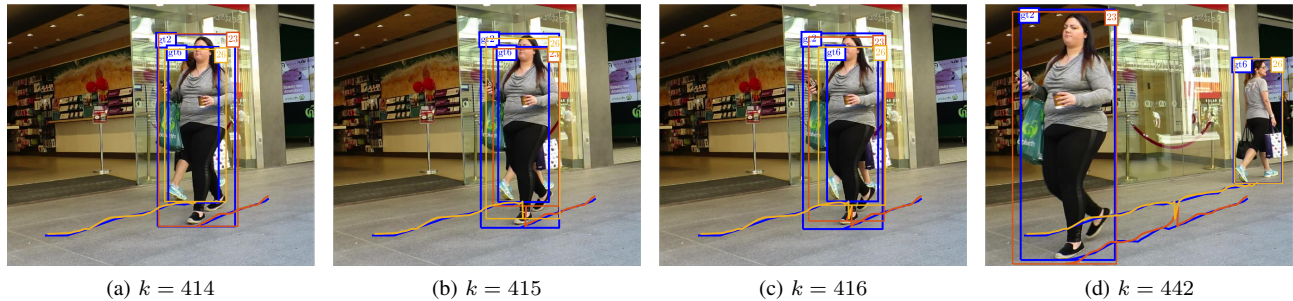


Fig. 4: BoT_SORT tracker results. The estimates switch positions at time step $k=415$, see Figure 4b.



Fig. 5: GMPHDOG17 tracker results. Estimates are of lower-quality for the pedestrian $gt6$ when it is occluded.

considered algorithms are given in Table I. It can be seen that MOTA and IDF1 scores fail to show any difference between the BoT_SORT and GMPHDOG17 algorithms. This outcome is undesirable because the scores should reflect the different results of the algorithms differently. Nevertheless, the HOTA score could sort the algorithms based on their performance. While HOTA works well in this scenario, its weaknesses follow.

HOTA can be understood as combining two separate scores for detection and association. For clarity, its definition is included in Appendix. In [10], HOTA compares favorably with scores such as MOTA and IDF1, addressing their various drawbacks. However, as we will demonstrate, HOTA still exhibits several undesirable behaviors. First, HOTA is not, as claimed in [10], a mathematically well-defined metric. A mathematically sound metric should satisfy four properties: 1) the distance from a point to itself is zero, 2) positivity, 3) symmetry, and 4) triangle inequality. It is clear that HOTA does not satisfy property 1) as it is a score such that the higher the value, the better, and the HOTA between a point to itself is one. The triangular inequality is not met either, which is further illustrated in Section VII. Second, in the HOTA calculation, the ground truth-to-estimate assignment problems are individually solved at each time step (frame). While this lowers the computational complexity, it is a heuristic solution as the 2D assignment problems are sequentially connected due to temporal correlation. Principled solutions should be obtained by (approximately) solving a multi-dimensional assignment problem, see [14]. Third, HOTA does not capture the localization accuracy explicitly, which needs to be represented using another score LocA [10]. Last,

HOTA is calculated by averaging multiple scores over multiple localization thresholds for solving the different 2D assignment problems. The averaging process was introduced to account for the localization accuracy in [10], which is arguably not an elegant solution⁴.

This section demonstrated that CV scores may have problems distinguishing the performance of several algorithms and do not possess the properties of a metric. The following section presents a mathematically sound performance evaluation score that is mathematically a metric and shows how it can be used efficiently to evaluate visual tracking algorithms and beyond.

IV. The TGOSPA Metric

The *trajectory generalized optimal sub-pattern assignment* (TGOSPA) is a metric on the space of sets of discrete-time trajectories, originally introduced in [14]. First, the notation is introduced, followed by the definition of the TGOSPA metric. The TGOSPA metric has several parameters that need to be selected prior to its use, which are discussed next. After revealing the general meaning of the parameters, their detailed choice for the case of CV applications follows.

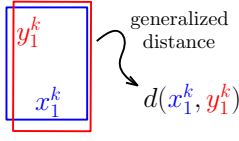
A. Notation and TGOSPA metric Definition

Let (\mathcal{X}, d) be a metric space⁵. Note that d is a metric, i.e., a function that assigns the *distance* $d(x, y)$ to a pair of elements $x, y \in \mathcal{X}$, such as the Euclidean distance. The elements of \mathcal{X} are referred to as object instances, and they represent bounding boxes in the CV setting of this paper. In particular, bounding boxes can be represented both as geometric entities (axis-aligned rectangle $x \subset \mathbb{R}^4$) or as vectors (e.g., using the center point

⁴The tracking accuracy for thresholds in the range $\{0.05, 0.1, \dots, 0.95\}$ are all treated as equally important, which is questionable.

⁵Note that this paper uses a slightly more general formulation than that in [14], [15] where it is assumed that $\mathcal{X} = \mathbb{R}^n$. It can be seen that TGOSPA has the same properties as derived in [14], [15] with (\mathcal{X}, d) being any metric space. Moreover, TGOSPA can be extended for random sets of trajectories assuming further that (\mathcal{X}, d) is complete and separable, i.e., is consistent with the random (finite) set formulation [25] that requires \mathcal{X} to be equipped with a locally compact, Hausdorff and second countable topology.

$[c_1^x \ c_2^x]^\top$, width w^x and height h^x as $x=[c_1^x \ c_2^x \ w^x \ h^x]^\top$.



A possible choice of the metric d in this setting is $d(x, y) = 1 - \text{IoU}(x, y)$, where $\text{IoU}(x, y)$ is the intersection over union (IoU) of the two bounding boxes x and y [26].

Let $k=0$ be the initial (i.e., first) time step and $K>0$ be the final time step. A trajectory $X \in \mathcal{T}(\mathcal{X})$ corresponding to some possibly moving object is a sequence of elements of \mathcal{X} together with time steps that indicate when the elements are present. For instance, a trajectory that is comprised of a single *segment* can have the form $X = (k_s, [x^{k_s} \ x^{k_s+1} \ \dots \ x^{k_s+\nu-1}])$, where k_s is the start-time with $0 \leq k_s \leq K$, ν is the duration (length) and $[x^{k_s} \ x^{k_s+1} \ \dots \ x^{k_s+\nu-1}]$ is the sequence of consecutive elements of \mathcal{X} (i.e., the object instances) that are indexed by the time step $k \in \{k_s, k_s+1, \dots, k_s+\nu-1\}$. In general, trajectories can have *gaps*, i.e., the object instances need not appear consecutively in time. This can be addressed straightforwardly by appending several segments together, see [14, Sec. II.A] for details. To access individual elements of a trajectory composed of a single segment, let τ^k be the set-valued function that returns the set with the element at time step k if it exists, or the empty set as

$$\mathbf{x}^k = \tau^k(X) = \begin{cases} \{x^k\} & \text{if } k_s \leq k \leq k_s + \nu - 1, \\ \emptyset & \text{otherwise.} \end{cases} \quad (1)$$

Multiple trajectories are modeled as a set of trajectories $\mathbf{X} = \{X_1, \dots, X_{|\mathbf{X}|}\} \in \mathcal{F}(\mathcal{T}(\mathcal{X}))$, where $\mathcal{F}(\cdot)$ denotes the collection of all finite subsets of the input set, with $|\cdot|$ denoting the cardinality. To access the set of object instances within \mathbf{X} that are present at time step k , τ^k is generalized to sets of trajectories as

$$\tau^k(\mathbf{X}) = \bigcup_{X \in \mathbf{X}} \tau^k(X). \quad (2)$$

Indeed, the TGOSPA metric is a metric on $\mathcal{F}(\mathcal{T}(\mathcal{X}))$ [14, Appendix B.A], i.e., it formalizes the distance between two sets of trajectories $\mathbf{X} = \{X_1, \dots, X_{|\mathbf{X}|}\}$ and $\mathbf{Y} = \{Y_1, \dots, Y_{|\mathbf{Y}|}\}$. For performance evaluation, one of the sets (e.g., \mathbf{X}) contains ground truth data, while the other (e.g., \mathbf{Y}) contains estimated trajectories.

In the computation of TGOSPA, trajectories from \mathbf{X} and \mathbf{Y} are assigned to each other at each time step, for which auxiliary notation is needed. Let $\Pi_{\mathbf{X}, \mathbf{Y}}$ be the set of all assignment vectors between the index sets $\{1, \dots, |\mathbf{X}|\}$ and $\{0, \dots, |\mathbf{Y}|\}$ that maps trajectories to each other at each time step as follows. At any time step k , an assignment vector $\pi^k = [\pi_1^k, \dots, \pi_{|\mathbf{X}|}^k]^\top$ describes the assignment of each trajectory in \mathbf{X} to a trajectory in \mathbf{Y} at time step k , with the index $\pi_i^k \in \{0, \dots, |\mathbf{Y}|\}$. The value $\pi_i^k = 0$ means that the trajectory i is unassigned at time step k and $\pi_i^k = j > 0$ means that the trajectory i is assigned to trajectory Y_j at time step k . At each time step, each trajectory in \mathbf{X} can be assigned to at most one trajectory \mathbf{Y} , which is expressed by the implication $(\pi_i^k = \pi_j^k > 0) \Rightarrow (i = j)$. Let $\pi^{0:K} = [\pi^0, \dots, \pi^K] \in \{0, \dots, |\mathbf{Y}|\}^{|\mathbf{X}| \times K}$ be the matrix containing the assignments vectors across all

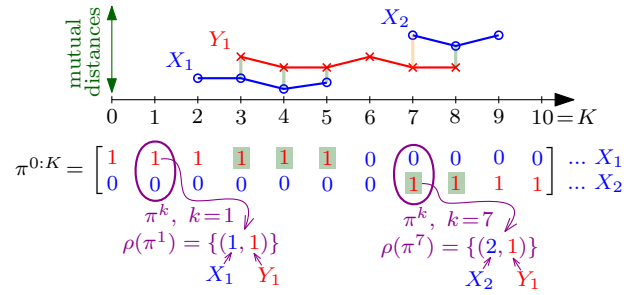


Fig. 6: Example assignment matrix $\pi^{0:K}$ for two sets of trajectories $\mathbf{X} = \{X_1, X_2\}$ depicted in blue and $\mathbf{Y} = \{Y_1, Y_2\}$ depicted in red. For instance, the trajectories X_2 and Y_1 are assigned at $k = 7$, which is indicated by $\rho(\pi^7) = \{(2, 1)\}$. Similarly, the trajectories X_1 and Y_1 are assigned at $k = 1$, which is indicated by $\rho(\pi^1) = \{(1, 1)\}$, although neither of the objects are present at $k = 1$.

time steps. To directly access the indices of the trajectories that are paired at time step k , let $\rho(\pi^k)$ denote the set of pairs $(i, j) \in \rho(\pi^k)$, such that that trajectory i is assigned to trajectory j at time step k . Note that two trajectories can be assigned to each other at any time step, i.e., even at time steps when one (or both) of the trajectories have no object instance present (e.g., did not start yet, or has already ended). The assignments in $\pi^{0:K}$ being encoded with ρ are *trajectory-level* assignments, and their temporal changes are key to assessing track changes present in the data. Example assignments are given in Fig. 6.

If two trajectories X_i and Y_j are assigned at a particular time step k , their mutual distance at that time step is computed as follows. First, the object instances at the time step k are extracted from the trajectories with

$$\mathbf{x}_i^k = \tau^k(X_i), \quad (3a)$$

$$\mathbf{y}_j^k = \tau^k(Y_j). \quad (3b)$$

Then, for $1 \leq p < +\infty$ and cut-off parameter $c > 0$, the distance between the sets \mathbf{x}_i^k and \mathbf{y}_j^k is computed by

$$d_p^{(c)}(\mathbf{x}_i^k, \mathbf{y}_j^k) = \begin{cases} \min(c, d(x_i^k, y_j^k)) & \mathbf{x}_i^k = \{x_i^k\}, \mathbf{y}_j^k = \{y_j^k\}, \\ 0 & \mathbf{x}_i^k = \mathbf{y}_j^k = \emptyset, \\ \frac{c}{\sqrt{2}} & \text{otherwise.} \end{cases} \quad (4)$$

In fact, $d_p^{(c)}$ in (4) is a special case of the GOSPA metric [27] between the sets \mathbf{x}_i^k and \mathbf{y}_j^k that both have at most one element [14, Sec. II.B]. Note that the first case of the definition of $d_p^{(c)}$ in (4), i.e., $d_p^{(c)}(\{x_i^k\}, \{y_j^k\}) = \min(c, d(x_i^k, y_j^k))$ is a *cut-off* metric.

The following definition of the TGOSPA metric emphasizes that even non-existing trajectories may be assigned. Such a definition is beneficial for understanding how the metric assesses track changes. The straightforward use of ρ in the following definition leads to a slightly different notation than the original TGOSPA metric definition [14].

Definition 1 (TGOSPA metric): Let $1 \leq p < +\infty$, cut-off parameter $c > 0$ and switching penalty $\gamma > 0$ be given real numbers (the TGOSPA parameters). The TGOSPA metric

between two sets of trajectories \mathbf{X}, \mathbf{Y} is defined by

$$d_p^{(c,\gamma)}(\mathbf{X}, \mathbf{Y}) = \min_{\pi^{0:K} \in \Pi_{\mathbf{X}, \mathbf{Y}}^{K+1}} \left(\underbrace{A(\mathbf{X}, \mathbf{Y}, \pi^{0:K})}_{\mathbf{X}, \mathbf{Y}\text{-assigned term}} + \underbrace{\gamma^p S(\pi^{0:K})}_{\text{switch term}} + \underbrace{\frac{c^p}{2} U(\mathbf{X}, \pi^{0:K})}_{\mathbf{X}\text{-unassigned term}} + \underbrace{\frac{c^p}{2} U(\mathbf{Y}, \pi^{0:K})}_{\mathbf{Y}\text{-unassigned term}} \right)^{1/p}, \quad (5)$$

where, respectively,

$$A(\mathbf{X}, \mathbf{Y}, \pi^{0:K}) = \sum_{k=0}^K \sum_{(i,j) \in \rho(\pi^k)} d_p^{(c)}(\mathbf{x}_i^k, \mathbf{y}_j^k)^p, \quad (6a)$$

$$S(\pi^{0:K}) = \sum_{k=0}^{K-1} \sum_{i=1}^{|\mathbf{X}|} s(\pi_i^k, \pi_i^{k+1}), \quad (6b)$$

$$U(\mathbf{X}, \pi^{0:K}) = \sum_{k=0}^K (|\tau^k(\mathbf{X})| - |\rho(\pi^k)|), \quad (6c)$$

are the \mathbf{X}, \mathbf{Y} -assigned term, number of switches and the number of object instances⁶ from \mathbf{X} that are left unassigned (analogously to \mathbf{Y}). For simplicity, the dependency of $A(\mathbf{X}, \mathbf{Y}, \pi^{0:K})$ (6a) on p and c is omitted. For a trajectory in \mathbf{X} with the index i , switches are counted based on temporal changes in the associations as

$$s(\pi_i^k, \pi_i^{k+1}) = \begin{cases} 0 & \pi_i^k = \pi_i^{k+1}, \\ 1 & \pi_i^k \neq \pi_i^{k+1}, \pi_i^k \neq 0, \pi_i^{k+1} \neq 0, \\ \frac{1}{2} & \text{otherwise.} \end{cases} \quad (7)$$

The second and the third case of the $s(\pi_i^k, \pi_i^{k+1})$ (7) definition will be referred to as *full*- and *half*-switches, respectively. The symbol $\pi_*^{0:K}$ denotes the argument of minimum of (5). \square

The TGOSPA metric computation is, unfortunately, an NP-hard problem. Therefore, approximations are required for large-scale problems involving many trajectories [14], [28]. In practical examples and the Python and Matlab implementations available at this link^{7,8}, an approximation based on the linear programming (LP) formulation is used [14, Sec. IV.B]. The resulting approximation is also a metric, referred to as the *LP metric*, and serves as an accurate lower bound for the TGOSPA metric. Therefore, the discussion focuses on the TGOSPA metric instead of the LP metric in the following.

It can be seen that the metric classifies the data \mathbf{X} and \mathbf{Y} into four terms depending on the parameters c , p , and γ . In the following, the classification terms are treated first. The parameters are explained subsequently.

B. TGOSPA Metric Decomposition

The four terms the data get classified into by TGOSPA correspond to indices where $\pi^{0:K}$ is non-zero (\mathbf{X}, \mathbf{Y} -assigned term), zero (\mathbf{X} -unassigned and \mathbf{Y} -unassigned

terms⁹) and to how $\pi^{0:K}$ changes in time for each row (Switch term). To make a good sense of the terminology regarding "missed" and "false" objects in the following, let \mathbf{X} represent the set of ground truth trajectories and \mathbf{Y} the set of estimated trajectories. Note, however, that their roles can be interchanged since TGOSPA is a metric.

1. Illustrative Example

Consider the example given in Fig. 6 and assume that the depicted assignment matrix $\pi^{0:K}$ is the argument of the TGOSPA minimum $\pi_*^{0:K}$ for some parameters p , c and γ . In that case, $A(\mathbf{X}, \mathbf{Y}, \pi^{0:K})$ (6a) is the sum of the distances highlighted in green (assuming each of them is smaller than c) and $\frac{c^p}{2} \times 2 = c^p$ due to 1) the trajectory X_1 assigned to Y_1 at $k=2$, where Y_1 has no object instance, and 2) the trajectory X_2 assigned to Y_1 at $k=9$, where Y_1 has no object instance neither. If moreover 3) the value of c were such that $\min(c, d(x_2^7, y_1^7)) = c$ at $k=7$, then the corresponding summand in $A(\mathbf{X}, \mathbf{Y}, \pi^{0:K})$ (6a) would be c^p . In addition, the \mathbf{X} -unassigned term is zero and the \mathbf{Y} -unassigned term counts $\frac{c^p}{2}$ once because the trajectory Y_1 is unassigned at $k=6$. Furthermore, there would be two half-switches weighted by γ^p in the switch term, i.e., one switch in total.

In the context of performance evaluation, it is more convenient to view the three TGOSPA terms (\mathbf{X}, \mathbf{Y} -assigned, \mathbf{X} - and \mathbf{Y} -unassigned terms) from the perspective of *properly estimated*, missed and false object instances regardless of their assignments. For the example described above, the properly detected object instances are those giving rise to the summands in $A(\mathbf{X}, \mathbf{Y}, \pi^{0:K})$ (6a) that are *not* due to 1), 2) and also 3). The summands in $A(\mathbf{X}, \mathbf{Y}, \pi^{0:K})$ (6a) that are due to 1), 2) and "one half" of 3), i.e., $\frac{c^p}{2}$ would constitute the missed objects term. The "second half" of 3), i.e., $\frac{c^p}{2}$ together with \mathbf{Y} -unassigned term would constitute the false alarms terms. The switch cost would stay the same.

2. Decomposition Suitable for Performance Evaluation

The localization term corresponds to properly estimated objects by counting the actual distances. Properly estimated object instances constitute the pairs x_i^k, y_j^k for which the corresponding summands in $A(\mathbf{X}, \mathbf{Y}, \pi^{0:K})$ (6a) are the distances to the p -th power $d(x_i^k, y_j^k)^p$ which are lower than c^p . To directly access the indices of properly estimated trajectories at time step k , let $\theta_k^{(c)}(\mathbf{X}, \mathbf{Y}, \pi^k) \subset \rho(\pi^k)$ denote the set of pairs

$$\theta_k^{(c)}(\mathbf{X}, \mathbf{Y}, \pi^k) = \{(i, j) \in \rho(\pi^k) : \mathbf{x}_i^k = \{x_i^k\}, \mathbf{y}_j^k = \{y_j^k\} \text{ and } d(x_i^k, y_j^k) < c\}. \quad (8)$$

The assignments in $\pi^{0:K}$ that are extracted via θ are *object instance-level* assignments and are key for the TGOSPA

⁶The function (6c) counts object instances within trajectories that are left unassigned over time, not entire trajectories.

⁷Python: github.com/Agarciafernandez/T-GOSPA-metric-python

⁸Matlab: github.com/Agarciafernandez/MTT

⁹The \mathbf{X} -unassigned term is eventually the number of indices where $\pi^{0:K}$ is zero, multiplied by $\frac{c^p}{2}$. For each time step, the number where $\pi^{0:K}$ is nonzero (i.e., $|\rho(\pi^k)|$) is subtracted from the maximum possible number (i.e., $|\tau^k(\mathbf{X})|$). The \mathbf{Y} -unassigned term is also the number of indices where $\pi^{0:K}$ is zero (multiplied by $\frac{c^p}{2}$), but for the case when \mathbf{X} and \mathbf{Y} are interchanged, i.e., for $\pi^{0:K} \in \Pi_{\mathbf{Y}, \mathbf{X}}$.

metric decomposition. The distances, i.e., the localization term, is then given by

$$L_p^{(c)}(\mathbf{X}, \mathbf{Y}, \pi^{0:K}) = \sum_{k=0}^K \sum_{(i,j) \in \theta_k^{(c)}(\mathbf{X}, \mathbf{Y}, \pi^k)} d_p^{(c)}(\mathbf{x}_i^k, \mathbf{y}_j^k)^p \quad (9)$$

The number of properly estimated objects is the number of summands in (9), and is denoted as

$$N^{(c)}(\mathbf{X}, \mathbf{Y}, \pi^{0:K}) = \sum_{k=0}^K |\theta_k^{(c)}(\mathbf{X}, \mathbf{Y}, \pi^k)|. \quad (10)$$

The remaining summands in $A(\mathbf{X}, \mathbf{Y}, \pi^{0:K})$ (6a) correspond to missed and false object instances. The number of such remaining objects are all weighted by $\frac{c^p}{2}$ and are to be *split* into $U(\mathbf{X}, \pi^{0:K})$ (6c) and $U(\mathbf{Y}, \pi^{0:K})$ (6c).

Consider the sets of missed and false object instances stored as tuples, containing the time step and the trajectory index i or j that is either missed or false,

$$\mathcal{M}(\mathbf{X}, \mathbf{Y}, \pi^{0:K}) = \{(k, i): \nexists j: (i, j) \in \theta_k^{(c)}(\mathbf{X}, \mathbf{Y}, \pi^k), \mathbf{x}_i^k = \{\mathbf{x}_i^k\}\}, \quad (11)$$

$$\mathcal{F}(\mathbf{X}, \mathbf{Y}, \pi^{0:K}) = \{(k, j): \nexists i: (i, j) \in \theta_k^{(c)}(\mathbf{X}, \mathbf{Y}, \pi^k), \mathbf{y}_j^k = \{\mathbf{y}_j^k\}\}, \quad (12)$$

respectively, with k ranging over $\{0, 1, \dots, K\}$, i ranging over $\{1, \dots, |\mathbf{X}|\}$ and j ranging over $\{1, \dots, |\mathbf{Y}|\}$. For simplicity, the dependency of $\mathcal{M}(\mathbf{X}, \mathbf{Y}, \pi^{0:K})$ (11) and $\mathcal{F}(\mathbf{X}, \mathbf{Y}, \pi^{0:K})$ (12) on p and c is omitted. Indeed, the numbers of properly detected, missed, and false object instances are the cardinalities of these sets. With this, the TGOSPA metric can be written as [14]

$$d_p^{(c, \gamma)}(\mathbf{X}, \mathbf{Y}) = \min_{\pi^{0:K} \in \Pi_{\mathbf{X}, \mathbf{Y}}^{K+1}} \left(\overbrace{L_p^{(c)}(\mathbf{X}, \mathbf{Y}, \pi^{0:K})}^{\text{localization term}} + \overbrace{\gamma^p S(\pi^{0:K})}^{\text{switch term}} \right) + \underbrace{\frac{c^p}{2} |\mathcal{M}(\mathbf{X}, \mathbf{Y}, \pi^{0:K})|}_{\text{missed objects term}} + \underbrace{\frac{c^p}{2} |\mathcal{F}(\mathbf{X}, \mathbf{Y}, \pi^{0:K})|}_{\text{false alarms term}} \Big)^{1/p}. \quad (13)$$

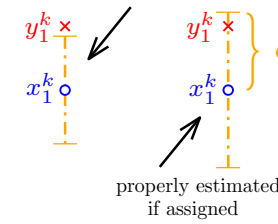
To see how TGOSPA classifies into $L_p^{(c)}(\mathbf{X}, \mathbf{Y}, \pi^{0:K})$ (9), $S(\pi^{0:K})$ (6b), $\mathcal{M}(\mathbf{X}, \mathbf{Y}, \pi^{0:K})$ (11), $\mathcal{F}(\mathbf{X}, \mathbf{Y}, \pi^{0:K})$ (12), the parameters p , c and γ need to be explained.

C. General Meaning of TGOSPA Parameters

It can be seen that the distances counted in the localization term $L_p^{(c)}(\mathbf{X}, \mathbf{Y}, \pi^{1:K})$ (9) are a *cut-off* dis-

tances, i.e., each term in (9) is always smaller than c^p .

surely false/missed objects

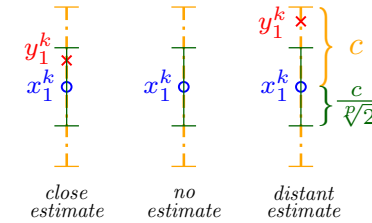


That is, c is the maximum localization error between a ground truth object and its estimate such that the ground truth *can* be counted as properly estimated. If an estimate is at a distance greater than c , the ground truth object and the estimate

constitute a pair of missed/false object instances, and both are weighted with $\frac{c^p}{2}$. If two trajectories are assigned to each other but there is no object instance at a particular time step in one of the trajectories, the corresponding cost $\frac{c^p}{2}$ is counted within either the missed objects or false alarms term, depending on which one is missing.

Notice that the weight of both a false alarm and a missing estimate is the same¹⁰ and equal to $\frac{c^p}{2}$. As a result, enlarging the cut-off parameter c enlarges the weight of each false and missed target compared to the distance of any properly estimated object, which might be undesirable.

assume x_1^k and y_1^k are associated
i.e., $(1, 1) \in \theta^k(\pi^k)$



$$d_b(x_1^k, y_1^k)^p < \frac{c^p}{2} < d_b(x_1^k, y_1^k)^p$$

On the other hand, a *distant estimate* (an estimate farther than $\frac{c}{\sqrt[2]{2}}$ that is associated with the ground truth) leads to higher TGOSPA metric value than *no estimate*. As a result, setting c too small may lead to preferring algorithms that

are prone to missing objects over algorithms returning estimates (although more distant than $\frac{c}{\sqrt[2]{2}}$). The borderline value $\frac{c}{\sqrt[2]{2}}$ can be set closer to c by enlarging p .

The parameter $p \geq 1$, in general, penalizes outliers. That is, p characterizes the discrepancy between a *close* and *distant* estimate in the sense of the metric d . If $p=1$, localization errors are considered in a *uniform* manner. With an increasing value of p , estimates that are *close* to the ground truth become more and more indistinguishable relative to estimates that are more *distant* (but still closer than the value of c). With increasing p , the missed/false objects term earns a greater impact on the final value of the TGOSPA metric since the term of a pair of a missed and a false target is always larger than any of the terms in the localization term. If the value of the switching penalty γ is larger than c , the switch term earns a greater impact on the final value of the TGOSPA metric compared to all other terms with an increasing value of p .

The half-switches in (7) are introduced to ensure the symmetry of the metric, and they penalize assignment-to-unassignment temporal changes in rows of $\pi^{0:K}$. This implies that the number of switches $S(\pi_{\star}^{1:K})$ (6b) need not be an integer, see [14, Appendix A3]. The switching

¹⁰False and missing estimates are usually weighted the same in the CV scores as well, but often with number 1 instead of $\frac{c^p}{2}$ [10].

penalty γ sets the weight of a single switch to be γ^p . For $\gamma=0$, switches are not counted at all, and TGOSPA can be computed efficiently using the GOSPA metric (with parameter $\alpha=2$) [15, Sec. IV.C] at every single time step. TGOSPA with $\gamma=0$, however, is not a metric on the space of finite sets of trajectories¹¹. With an increasing number of γ , switches that *seemingly* exist in the data may or may not be counted. For extremely large values of $\gamma \rightarrow +\infty$, the switches become too costly to be present in $\pi_{\star}^{0:K}$ (i.e., counted as switches in the final TGOSPA value), and the estimates that are responsible for the track changes become counted as false alarms. TGOSPA metric with extremely large γ can be computed in a simplified manner in this case as well [15, Sec. IV.C]. Although this behavior might seem counter-intuitive, the following Section shows how the (nonzero and finite) value of γ can be interpreted geometrically alongside the other parameters. This, in turn, can be used to design γ conveniently.

D. Setup of the Switching Penalty

In this section, simple rules are derived such that short and long-term track changes are properly found and assessed within the TGOSPA metric as switches. The rules give rise to two general methods for conveniently selecting γ . To ease the notation, let $\mathbf{1}_{n \times m}$ be the matrix of ones and $\mathbf{0}_{n \times m}$ be the matrix of zeros, both $n \times m$.

1. Accounting for Short-term Interim Track Changes

Consider a scenario with two ground truth trajectories X_1 and X_2 and a single estimated trajectory Y_1 as shown in Fig. 7. Seemingly, there are two switches in the scenario. The first switch is because the trajectory Y_1 tracks X_1 before the time step $k=t$ and X_2 after that. The second switch appears because Y_1 subsequently switches back to track X_1 . Examples of two possible assignments that may optimize the TGOSPA criterion are as follows.

- *No switch*: The trajectory Y_1 is assigned to trajectory X_1 for all time instants, i.e., no switch occurs. The corresponding assignment matrix is $\pi_{\text{no switch}}^{0:K} = \begin{bmatrix} \mathbf{1}_{1 \times (K+1)} \\ \mathbf{0}_{1 \times (K+1)} \end{bmatrix}$.
- *Two switches*: The trajectory Y_1 is assigned to trajectory X_1 for all time instants *except* the time step t , at which it is associated with trajectory X_2 i.e., two switches occur as explained above. The corresponding assignment matrix is $\pi_{\text{two switches}}^{0:K} = \begin{bmatrix} \mathbf{1}_{1 \times t}, 0, \mathbf{1}_{1 \times (K-t)} \\ \mathbf{0}_{1 \times t}, 1, \mathbf{0}_{1 \times (K-t)} \end{bmatrix}$ that gives rise to four half-switches and thus $S(\pi_{\text{two switches}}^{0:K})=2$.

¹¹To see this, consider arbitrary estimation results and *connect* the estimates in time in two different ways to yield two different sets of trajectories. As the *connections* are not considered by TGOSPA with $\gamma=0$, the distance between the two sets is zero, although the trajectories are clearly different, violating the identity property of a metric. On the other hand, such a choice can be understood as computing the GOSPA metric for any individual time step, which is a metric on the space of finite sets of object instances [27].

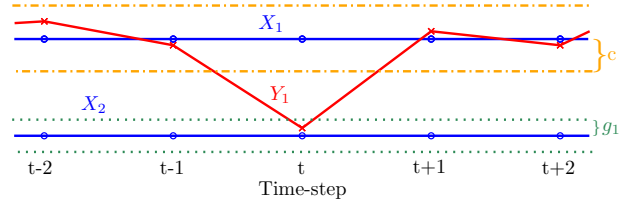


Fig. 7: Short-term track change scenario illustration. Assume that Y_1 is assigned to X_1 except for the time step t . For the indicated values of c and g_1 , there is a certain choice of γ according to (18) for some p . Ever since the distance $d(x_2^t, y_1^t)$ is less than g_1 , the scenario is considered as two switches: one due to Y_1 switching from X_1 to X_2 between $t-1$ and t , and one for switching back to X_1 between t and $t+1$.

Depending on the value of γ , assume that one of the above assignments minimizes the TGOSPA criterion, i.e., is equal to $\pi_{\star}^{0:K}$. The goal is to find the threshold value of γ and corresponding geometrical conditions, for which the assignments are equally evaluated by the TGOSPA terms.

As depicted in Fig. 7, assume that the value of c is such that¹² $d(x_1^t, y_1^t) > c$, i.e., assigning Y_1 to X_1 (which is the case for $\pi_{\text{no switch}}^{0:K}$) yields a pair of missed/false objects at the time step t . If the assignment matrix $\pi_{\text{no switch}}^{0:K}$ minimizes $\pi_{\star}^{0:K}$ for some γ , the p -th power of TGOSPA is

$$d_p^{(c, \gamma)}(\mathbf{X}, \mathbf{Y})^p = \sum_{k=0}^{t-1} \underbrace{\left(d(x_1^k, y_1^k)^p + \frac{c^p}{2} \right)}_{\substack{x_1^k \text{ is properly estimated with } y_1^k, \\ x_2^k \text{ is missed}}} + \underbrace{\frac{c^p}{2} \cdot (2+1)}_{\substack{\text{time step } t \\ x_1^t, x_2^t \text{ are missed,} \\ y_1^t \text{ is false}}} + \sum_{k=t+1}^K \left(d(x_1^k, y_1^k)^p + \frac{c^p}{2} \right). \quad (14)$$

If, on the contrary, it is the assignment matrix $\pi_{\text{two switches}}^{0:K}$ that minimizes $\pi_{\star}^{0:K}$ for some other γ , then

$$d_p^{(c, \gamma)}(\mathbf{X}, \mathbf{Y})^p = \sum_{k=0}^{t-2} \left(d(x_1^k, y_1^k)^p + \frac{c^p}{2} \right) + \underbrace{\left(d(x_1^{t-1}, y_1^{t-1})^p + \frac{c^p}{2} + \gamma^p \right)}_{\substack{\text{time step } t-1 \\ x_2^{t-1} \text{ is missed,} \\ \text{two half-switches}}} + \underbrace{\left(d(x_2^t, y_1^t)^p + \frac{c^p}{2} + \gamma^p \right)}_{\substack{\text{time step } t \\ x_1^t \text{ is missed,} \\ \text{two half-switches}}} + \sum_{k=t+1}^K \left(d(x_1^k, y_1^k)^p + \frac{c^p}{2} \right), \quad (15)$$

The threshold for γ for which the assignments yield the same TGOSPA metric value is the one for which (14) and (15) are equal, i.e.,

$$\underbrace{\text{same terms}}_{\text{No switch case (14)}} + \frac{3c^p}{2} = \underbrace{\text{same terms}}_{\text{Two switches case (15)}} + d(x_2^t, y_1^t)^p + \frac{c^p}{2} + 2\gamma^p, \quad (16)$$

where the same terms refer to $\sum_{k=0}^{t-1} \left(d(x_1^k, y_1^k)^p + \frac{c^p}{2} \right)$ and $\sum_{k=t+1}^K \left(d(x_1^k, y_1^k)^p + \frac{c^p}{2} \right)$. That is, TGOSPA consid-

¹²The value of $1 \leq p < +\infty$ can be chosen arbitrarily. This holds in the next Section for long-term track changes as well.

ers the scenario as a switch if and only if (iff)

$$\gamma < \left(\frac{c^p - d(x_2^t, y_1^t)^p}{2} \right)^{1/p}. \quad (17)$$

In practice, one can select a threshold distance $g_1 < c$ for $d(x_2^t, y_1^t)$ that defines the boundary between the *no switch* and *two switches* assignments. For a given g_1 , switching penalty γ can be computed as

$$\gamma = \left(\frac{c^p - g_1^p}{2} \right)^{1/p}. \quad (18)$$

From (17) it follows that whenever $d(x_2^t, y_1^t) < g_1$, the scenario is considered as a switch in TGOSPA. Vice-versa, if γ is selected such that $\gamma < \frac{c}{\sqrt[2]{p}}$, there exists g_1 such that

$$g_1 = (c^p - 2\gamma^p)^{1/p}. \quad (19)$$

An example of g_1 is depicted in Fig. 7, for which the scenario is considered a switch in TGOSPA. Notice that the value of γ (18) is rather small when selected via $g_1 < c$, i.e., $\gamma \in (0, \frac{c}{\sqrt[2]{p}})$. Accounting for short-term interim track changes by selecting γ is thus indicated in this paper with the term **Gamma small**.

When γ is kept fixed, enlarging the parameter p enlarges the threshold distance g_1 (19) up to the (fixed) value of c . When p and c are kept fixed, enlarging g_1 lowers the value of γ (18) and thus the penalty of a switch.

Setting g_1 and computing γ using (18) is a convenient method for selecting γ due to the simple graphical interpretation of g_1 . However, if there are more estimates/ground truth trajectories and/or the value of c is considerably larger than the one depicted in Fig. 7 (or the ground truth objects are considerably closer to each other), the interpretation of γ using g_1 described above is no longer valid.

Note that the subscript 1 in g_1 indicates the concern about assigning the estimated trajectory Y_1 to X_2 for *one* time step. The following section considers multiple time steps for a slightly altered scenario where the track change is permanent instead of interim.

Since γ (18) is small if set up via $g_1 < c$, note that long-term switches discussed next are considered as switches in this case as well. In many applications, however, it is desirable to penalize switches in the data with a larger weight. It follows that when setting γ so large that g_1 (19) no longer exists, no short-term switches will be found in the data. On the other hand, certain track changes (e.g., due to occlusion) will still be found in the data and will be penalized with the (large) value of γ . The next section establishes the details regarding such larger values of γ .

2. Accounting for Long-term Track Changes

Consider a scenario with two ground truth trajectories X_1 and X_2 and a single estimated trajectory Y_1 as shown in Fig. 8. Seemingly, there is a single switch in the scenario because the trajectory Y_1 tracks X_1 before the time step $k=t$, but then it switches to track X_2 . The trajectory Y_1 then tracks X_1 for $\ell=3$ time steps, after which the trajectory Y_1 terminates. Assuming that Y_1 gets

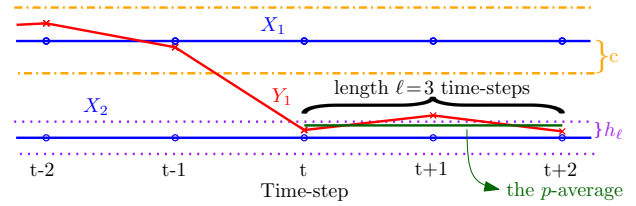


Fig. 8: Long-term track change scenario illustration.

assigned to X_1 for $k=0, \dots, t-1$, it suffices to consider the following two assignments.

- *No switch*: The trajectory Y_1 is assigned to trajectory X_1 for all time instants i.e., no switch occurs. The corresponding assignment matrix is $\pi_{\text{no switch}}^{0:K} = \begin{bmatrix} \mathbf{1}_{1 \times (K+1)} \\ \mathbf{0}_{1 \times (K+1)} \end{bmatrix}$.
- *One switch*: The trajectory Y_1 is assigned to trajectory X_1 only for $k=0, \dots, t-1$, after which it gets assigned to the trajectory X_2 . The corresponding assignment matrix is $\pi_{\text{one switch}}^{0:K} = \begin{bmatrix} \mathbf{1}_{1 \times t}, & \mathbf{0}_{1 \times (K-t+1)} \\ \mathbf{0}_{1 \times t}, & \mathbf{1}_{1 \times (K-t+1)} \end{bmatrix}$.

Depending on γ , it is assumed either one of the above assignments minimizes TGOSPA. As depicted in Fig. 8, assume that the value of c is such that $d(x_1^t, y_1^t) > c$, i.e., assigning Y_1 to X_1 (which is the case for $\pi_{\text{no switch}}^{0:K}$) yields a pair of missed/false objects at the time step t .

Again, the threshold value of γ , for which the assignments yield the same TGOSPA metric value, is the one for which $\pi_{\text{no switch}}^{0:K}$ and $\pi_{\text{one switch}}^{0:K}$ yield equal (minimum) value of TGOSPA. Since the derivation follows the same steps as for the interim track changes, only the result is given. It follows that TGOSPA considers the scenario as a switch iff

$$\gamma < \left(\ell \cdot c^p - \sum_{k=t}^{t+\ell-1} d(x_2^k, y_1^k)^p \right)^{1/p}, \quad (20)$$

where ℓ is the number of time steps between t and the end-time of Y_1 (assuming Y_1 tracks X_2 until it ends), further referred to as the *length of the track change*. In the example depicted in Fig. 8, the value of ℓ is 3. It can be seen that one can select a threshold distance $h_\ell < c$ that defines the boundary between the *no switch* and *one switch* assignments. For a given h_ℓ , the switching penalty γ can be computed as

$$\gamma = \left(\ell \cdot c^p - \ell \cdot h_\ell^p \right)^{1/p}. \quad (21)$$

From (20) it follows that whenever

$$\left(\frac{1}{\ell} \sum_{k=t}^{t+\ell-1} d(x_2^k, y_1^k)^p \right)^{1/p} < h_\ell, \quad (22)$$

p-average localization error of Y_1 w.r.t. X_2 (after the track change)

the scenario with the corresponding value of ℓ will be considered as a switch in TGOSPA. That is if the *p*-average localization error of Y_1 w.r.t. X_2 (after the switch) is lower than a predefined threshold distance h_ℓ . An example $h_\ell = h_3$ is depicted in Fig. 8, for which the scenario is considered as a switch in TGOSPA if, moreover, the corresponding *p*-average is such that (20) holds.

To account for track changes that are long *enough* only, one can select $n > 0$ and compute

$$\gamma = \sqrt[p]{n} \cdot c, \quad (23)$$

so that $h_\ell = 0$, for all $\ell = 1, 2, \dots, n$. In other words, any long-term track change that lasts for exactly $\ell = n$ time steps or less than n time steps will *not* be considered as a switch in TGOSPA. On the other hand, track changes that last longer still can be considered as switches in TGOSPA. In particular, combining (23) with (21) and (22), a track change lasting for $\ell = n + m$ time steps, $m > 0$, will be considered as a switch in TGOSPA iff

$$\left(\frac{1}{n+m} \sum_{k=t}^{t+n+m-1} d(x_2^k, y_1^k)^p \right)^{1/p} < h_{n+m} = \sqrt[p]{\frac{m}{n+m}} \cdot c, \quad (24)$$

(n is user-defined and $\ell = n + m$ is length of a real track change). For a fixed n , c and p , enlarging m enlarges the threshold distance h_{n+m} (24) up to c , i.e., track changes that last longer may have larger (p -average) localization error to be considered as switches. When n and c are fixed, enlarging p enlarges h_{n+m} for any $n, m > 0$.

Considering that n may be chosen arbitrarily large, the value of γ chosen using (23) can also be arbitrarily large. Accounting for long-term track changes by selecting γ is thus indicated in this paper with the term **Gamma large**. However, it should be emphasized that the assumption that Y_1 gets assigned to X_1 for $k = 0, \dots, t-1$ is crucial for the validity of the interpretation of (23). This assumption means that the estimated trajectory Y_1 first tracks X_1 for *sufficiently* large number of time steps with a *sufficient* accuracy. Setting $n > \frac{K+1}{2}$ (note that $K+1$ is the total number time steps) and computing γ (23) can be expected to make TGOSPA behave as if $\gamma \rightarrow +\infty$ since no track change could last for more than $\frac{K+1}{2}$ time steps.

Setting h_n and computing γ using (23) is a convenient method for selecting γ due to the simple graphical interpretation of h_n . Regarding short-term interim track changes, note that if there are more estimates/ground truth trajectories and/or the value of c is considerably larger (or the ground truth objects are considerably closer to each other), the interpretation of γ using h_n described above is no longer valid.

From the symmetry of the metric, note that the same rules apply if ground truth and estimates switch roles, i.e., for $\mathbf{X} = \{Y_1\}$ and $\mathbf{Y} = \{X_1, X_2\}$. Also note that one can *draw* the values of c , g_1 , h_ℓ , etc., relative to the estimates instead of the ground truth. Hence, it should be emphasized that the same choice of γ (23) applies for track fragmentation and thus for assessing occlusions. This is illustrated in Fig. 9 for one ground truth trajectory and two estimates that lead to one switch in TGOSPA.

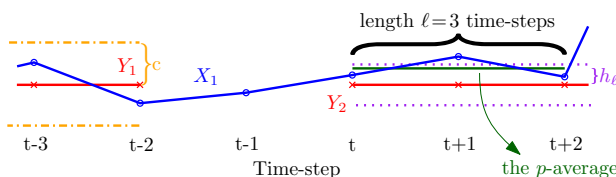


Fig. 9: Track fragmentation scenario illustration.

To sum up, the switching penalty $\gamma \in \left(0, \sqrt[p]{\frac{K+1}{2}} \cdot c\right)$ as explained in this subsection can be selected according to either one of the following two methods.

- **Gamma small: to find and penalize short-term interim track changes.** First, set the threshold distance g_1 such that $0 < g_1 < c$. Then compute $\gamma \leq \frac{c}{\sqrt[p]{2}}$ according to (18). Scenarios similar to those illustrated in Fig. 7 will be considered as two switches in TGOSPA whenever the real estimate will be such that $d(x_2^t, y_1^t) < g_1$.
- **Gamma large: to find and penalize long-term track changes lasting for at least $n+1$ time steps.** Compute $\gamma \geq c$ according to (23). Scenarios similar to those illustrated in Fig. 8 or 9 for the case $\ell = 3$ will be considered as one switch in TGOSPA whenever the real estimates will be such that (24) holds, i.e., if the p -average for the particular length of the switch $\ell = n + m$ is below h_{n+m} (24) for the chosen n .

It can be seen that given c and p , the penalty γ allows reflecting user preferences for the assessment of track changes *independently* of the application field (e.g., camera or radar tracking). The value of γ can be set indirectly through setting the parameter g_1 in the case of short-term interim track changes and n in the case of long-term track changes using (18) and (23), respectively. Moreover, setting $n > \frac{K}{2}$ results in TGOSPA behaving as if $\gamma \rightarrow +\infty$, and thus, no switches will be found in the data.

The following Section proposes a method for conveniently selecting the parameters p and c , including the metric d , which are specific for a given application. The CV setting of Section II will be used.

V. Application-dependent Parameters Selection

The parameters should be chosen properly to rank different algorithms depending on the application field and the user preferences. The first step is the selection of the metric d , which is discussed in the CV setting in this paper. Concise selection of the cut-off c together with the exponent parameter p follows next.

A. Selection of Metric for bounding boxes

As mentioned before, bounding boxes x, y may be represented as vectors (elements of \mathbb{R}^4) or as geometrical entities (subsets of \mathbb{R}^2). In the former case, common metrics such as the Euclidean or the maximum metrics¹³ can be readily used [26]. While the vector representation can be computed efficiently, the metric value depends on

¹³The maximum metric is defined as $d_\infty(x, y) = \max_i |x_i - y_i|$ for any desired vector-valued representation of a bounding box, with x_i being the i -th element of x .

the particular chosen description of the bounding box¹⁴. That is, the user has to choose parameters representing a bounding box for which the estimation error is computed.

The latter case of representation using geometric entities is free of a particular bounding box description¹⁵ and can have favorable geometric interpretations. Three particular metrics are discussed next.

1. Hausdorff Metric

Consider the sets $x, y \subset \mathbb{R}^2$ being non-empty and compact (i.e., closed and bounded). In general, the collection of non-empty compact subsets of the metric space $(d_{\mathbb{R}^n}, \mathbb{R}^n)$ can be made into a metric space¹⁶ by using the Hausdorff metric [30, p. 6], [29, pp. 137-138], denoted as $d_H(x, y)$. The Hausdorff metric generalizes the metric $d_{\mathbb{R}^n}$ on \mathbb{R}^n straightforwardly, as for any $\xi, \eta \in \mathbb{R}^n$, it is $d_H(\{\xi\}, \{\eta\}) = d_{\mathbb{R}^n}(\xi, \eta)$. Using the maximum metric $d_{\mathbb{R}^2}(\xi, \eta) = d_\infty(\xi, \eta)$, the Hausdorff metric can be computed easily for bounding boxes (rectangles containing their interiors) as [31]

$$d_H(x, y) = \max \left\{ \max\{|l_1^x - l_1^y|, |r_1^x - r_1^y|\}, \max\{|l_2^x - l_2^y|, |r_2^x - r_2^y|\} \right\}, \quad (25)$$

where l_i^x and r_i^x are the left and right end-points of the set x projected to the dimension i , respectively (analogically for y). The resulting Hausdorff metric (25) focuses solely on the mutual discrepancy between the *edges* of the bounding boxes and may thus ill-consider their overall geometric relationship.

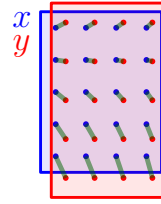
2. Wasserstein Metric

Consider the sets $x, y \subset \mathbb{R}^2$ being non-empty and measurable. Such sets can be understood as supports of probability density functions (PDFs), say, $p_x(\xi)$ and $p_y(\eta)$ with probability measures P_x and P_y , respectively. One can, in turn, define the Wasserstein metric $d_W(P_x, P_y)$ between the measures, which has a convenient interpretation: *the mean distance needed to transport the mass under one PDF curve into the other* [32].

¹⁴An element $x \in \mathbb{R}^4$ can be comprised of, e.g., the center, top-left or bottom-center point. To capture the extent of the box, the width and height can be used as well as their radius $\frac{\text{width}}{2}$ and $\frac{\text{height}}{2}$. A chosen metric d on \mathbb{R}^4 leads to different values for different representations of the same boxes.

¹⁵The width and height of a box are both naturally nonnegative, which is immanent to the geometric representation as a set. To respect this within the vector representation, however, one should restrict \mathbb{R}^4 to some subset.

¹⁶The resulting metric space is also consistent with the *hit-or-miss* topology used in the theory of random closed/finite sets [29, p. 138] commonly adopted in the multi-object estimation community.



average distance

Taking uniform distributions and the Euclidean metric $d_{\mathbb{R}^2}(\xi, \eta) = d_2(\xi, \eta)$ on \mathbb{R}^2 , the Wasserstein distance can be computed easily for bounding boxes (rectangles containing their interiors) [33]. The computation is the same as the Euclidean distance for the vector representation $x = [c_1^x \ c_2^x \ \frac{1}{\sqrt{12}}w^x \ \frac{1}{\sqrt{12}}h^x]^\top$, where $[c_1^x \ c_2^x]^\top$ is the center-point, w^x is the width and h^x is the height of the bounding box x (analogically for y), i.e., as

$$d_W(P_x, P_y) = \left[(c_1^x - c_1^y)^2 + \frac{1}{3} \left(\frac{w^x}{2} - \frac{w^y}{2} \right)^2 + (c_2^x - c_2^y)^2 + \frac{1}{3} \left(\frac{h^x}{2} - \frac{h^y}{2} \right)^2 \right]^{1/2}. \quad (26)$$

The above metrics depend on the *shapes*, as well as *sizes* (scales) of the input bounding boxes to the metric. That is, two boxes that are small (presumably in the background of the image) can be expected to have *smaller* metric value than two boxes that are large (presumably in the foreground) even though both pairs would *look* the same if scaled to the same width and height. This inconvenience is solved by the following metric.

3. IoU-induced Metric

The CV community makes extensive use of the IoU¹⁷ that is a *similarity score* defined as

$$\text{IoU}(x, y) = \frac{\text{Area}(x \cap y)}{\text{Area}(x \cup y)}, \quad (27)$$

which is equal to one if the bounding boxes (rectangles containing their interiors) x and y coincide and zero if they have no overlap at all. Otherwise, the IoU (27) measures the relative overlap of the sets. For convenience, the Area in (27) is taken as the Lebesgue measure, and the sets $x, y \subset \mathbb{R}^2$ are assumed to be non-empty and Lebesgue-measurable. With this, it is easy to show that the IoU (27) is scale-invariant¹⁸. The function defined as [26]

$$d_{\text{IoU}}(x, y) = 1 - \text{IoU}(x, y) \quad (28)$$

is thus also scale-invariant, it is moreover a metric¹⁹ and it will be called the IoU-induced metric in this paper. For its favorable properties, the IoU-induced metric is chosen as the metric d in the following considerations, but the other metrics could be readily used as well.

¹⁷Generalizations of the IoU exist in the literature, see, e.g., [34]–[36].

¹⁸The proof is a simple consequence of the scaling property of the Lebesgue measure [37, 2.20 Theorem (e)]: take the linear transformation in the theorem to be any nonzero scale. The division in (27) then makes the constant granted by the theorem cancel out.

¹⁹Assuming the sets x, y are non-empty and finite, and taking Area to be the cardinality, the function $d_{\text{IoU}}(x, y)$ was shown to be a metric in [38]. Namely, the triangle inequality was shown to hold for such $d_{\text{IoU}}(x, y)$. As the steps in [38] are valid for taking Area to be any sigma-finite measure (as far as the sets x, y are measurable and both have *finite* measure), the proof is valid for the Lebesgue measure and bounding boxes.

B. Selection of Cut-off and Exponent Parameters

Suitable values of c and p naturally depend on the application at hand. In some cases, the selection of c can be done directly depending on the maximum allowable localization distance such that a ground truth and an estimate can be considered assigned, e.g., for the evaluation in 3D space. In general, however, the selection may be challenging, e.g., for the evaluation in 2D space where the data are under the effect of the perspective projection. Although the IoU-induced metric d_{IoU} (28) mitigates the perspective projection effects, the additional selection of p is arguably rather unintuitive. Although the choices $p=1$ or $p=2$ seem *natural*, such choices may barely reflect application-dependent user preferences.

A method to select c based on data was presented²⁰ in [26]. In the following, the method from [26] is extended to fit into the performance evaluation setting of this paper, and a method for joint selection of c and p is proposed.

The main idea of the proposed method is to choose, analyze, and visualize sample data, forming the following three steps:

1. choose application-relevant sample data,
2. based on [26], process the data to form example distances in the context of the application,
3. jointly select c and p based on histogram count and, if possible, visual specimen of the distances.

1. Application-relevant Sample Data

First, data based on which the selection of c and p is to be analyzed must be chosen. (i) The data should include ground truth and estimated trajectories (perhaps from several algorithms and videos), (ii) The estimated trajectories are *diverse* enough to include both *good* and *bad* estimates (according to the user). (iii) The data should form a relevant sample for the application, for which the evaluation will be done with the selected c and p .

The scenario studied in this paper involves 2D bounding boxes resulting from pedestrians walking near a static camera, which is aligned approximately parallel with the ground. The particular scenario lasts only for 61 frames, involves only two pedestrians, and is taken from the MOT17-09 video for which the same description applies. It can be assumed that the data from the *entire* video MOT17-09 (ground truth and trajectory estimates from all the applied algorithms) fulfills all the above requirements.

2. Extension of the Method from [26]

Consider ground truth trajectories \mathbf{X} and estimated trajectories \mathbf{Y} produced by an algorithm for a certain video of the chosen data. Four so-called *guideline* functions were introduced in [26], whose argument is the cut-off c . For simplicity, only two of the guideline functions are considered here, namely (i) *total number of assignments* and (ii) *sum of the squared distances*. The guideline

functions are constructed upon assignments resulting from computing the GOSPA metric with $p=2$ at each single time step for different values of c , i.e., the assignments $\pi_{\star}^{0:K}|_2^{(c,0)}$ resulting from the computation of $d_2^{(c,0)}$ (5). In the terminology of this paper, the guideline function (i) is the number of properly estimated objects *for given* c , which is further shortened as

$$N(c) = N^{(c)}(\mathbf{X}, \mathbf{Y}, \pi_{\star}^{0:K}|_2^{(c,0)}), \quad (29)$$

and the guideline function (ii) is the localization term *for given* c , which is further shortened as

$$L(c) = L_2^{(c)}(\mathbf{X}, \mathbf{Y}, \pi_{\star}^{0:K}|_2^{(c,0)}). \quad (30)$$

In [26], it was argued that four subsequent intervals I_1, I_2, I_3 and I_4 of $c \geq 0$ can be determined based on the guideline functions, that can be summarized as follows.

- I_1 The number of assignments increases rapidly. Close estimates get assigned, most of which are seemingly *correct* and minimum are false alarms. The function $N(c)$ (29) can be expected to increase rapidly in this interval up to a certain level, indicating that most of the correct estimates have been assigned while minimum false alarms have been included, which is the right endpoint of I_1 . In $L(c)$ (30), a large number of small increments is expected for $c \in I_1$, and thus its values can be arbitrarily large, offering little information about I_1 .
- I_2 Only correct detections with the largest error get associated, while only a small number of false alarms are used. This interval includes convenient distance values that can be used in the evaluation as the cut-off c . The function $N(c)$ (29) should not change much in this interval (and also in the following intervals). Similarly, the value of $L(c)$ (30) can be expected nearly constant for $c \in I_2$.
- I_3 A Slow increase in the number of assignments is caused primarily by assigning distant estimates that are seemingly false alarms. As a result, $N(c)$ (29) should increase only occasionally, and whenever this happens, the distance is expected to be large. Therefore, $L(c)$ (30) can be expected to have large occasional increments indicating that distant false alarms are being associated.
- I_4 There are no more assignments possible in the data.

The expected behavior of the guideline functions is illustrated in Fig. 10, where $\text{diff}(f(c)) = f(c + \Delta c) - f(c)$, computes the increments of the function f , with $\Delta c > 0$ being a user-defined parameter (bin width).

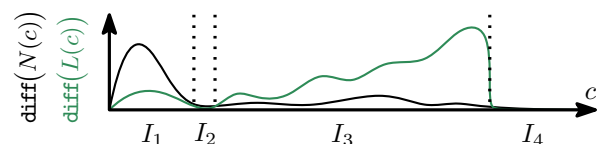


Fig. 10: Graphical sketch of expected properties of the increments of $N(c)$ (29) and $L(c)$ (30) taken from [26].

²⁰The paper [26] dealt with assigning detections to ground truth bounding boxes to estimate the measurement noise covariance matrix.

It should be pointed out that both functions $\text{diff}(N(c))$ (29) and $\text{diff}(L(c))$ (30) can be efficiently approximated via computing the histogram of $L(c_{\max})$ (30) summands $\{d(x_i^k, y_j^k)\}_{k,i,j}$ for a single large value c_{\max} , as

$$\text{diff}(N(c)) \approx \text{histogram}\left[\{d(x_i^k, y_j^k)\}_{k,i,j}\right](c), \quad (31)$$

$$\text{diff}(L(c)) \approx \text{diff}(N(c)) \cdot \text{bin_center}(c)^2, \quad (32)$$

where $\text{bin_center}(c)$ is the center of the bin of the computed histogram (31) closest to the value of c . Moreover, one can use the set of summands $\{d(x_i^k, y_j^k)\}_{k,i,j}$ collected from multiple algorithms and/or videos chosen for the selection of c and p to compute $\text{diff}(N(c))$ (31) and $\text{diff}(L(c))$ (32).

Using the IoU-induced metric $d=d_{\text{IoU}}$ (27), the value $c_{\max}=1$ can readily be used. The guideline functions computed from all the algorithms applied to the MOT17-09 video are shown in Fig. 11, where the intervals I_1 , I_2 , I_3 and I_4 were determined by hand based on the expected behavior (Fig. 10).

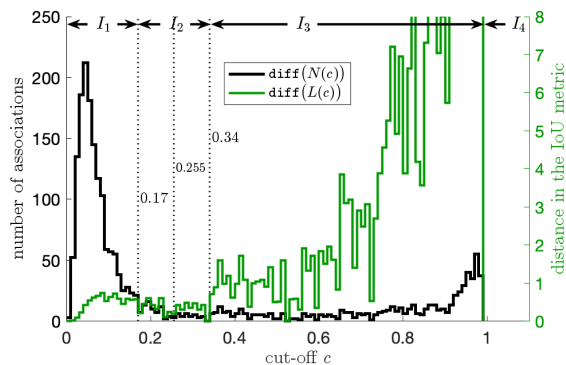


Fig. 11: Increments of the guideline functions $\text{diff}(N(c))$ (31) and $\text{diff}(L(c))$ (32) for the entire MOT17-09 video and sample distances collected from all the algorithms described in Section II.

At this point, the sample distances $\{d(x_i^k, y_j^k)\}_{k,i,j}$ from the data (multiple algorithms/videos) have been ordered from the smallest to the largest. If possible, the distances should be visualized in the context of the application²¹ including the bounding box pairs x_i^k, y_j^k giving rise to the distance $d(x_i^k, y_j^k)$. For the exemplary case, the visualization is given in Fig. 12.

3. Joint Selection of c and p

As discussed above, the cut-off c can be viewed as the maximum *possible* error for an estimate to be considered proper. The convenient value of c for the chosen data should lie in the interval I_2 , and its particular selection is made by the user (by hand) ideally with the help of the data visualization such as in Fig. 12.

At the same time, the value $a=\frac{c}{\sqrt[3]{2}}$ can be understood as a maximum *admissible* error such that the further

²¹The visualization should respect the ordering and disregard the information about the algorithm that produced the particular estimate.

estimates are penalized in TGOSPA more compared to the case of missing estimate (see Section C). As a is a distance, the user can easily select $a \in (\frac{c}{2}, c)$ similarly to selecting c from the data. The exponent parameter $p \geq 1$ can then be computed as

$$p = \frac{\log(2)}{\log(c) - \log(a)}, \quad (33)$$

which concludes the proposed method.

It is important to note that step 3. may be sufficient on its own for some applications, e.g., for the evaluation in 3D with the Euclidean distance where c and a can be chosen without relying on a particular dataset.

Three possible selections of c and p , suitable for different applications, are discussed in the following section, together with the performance evaluation of algorithms in the discussed CV scenario.

VI. Numerical Examples

In this Section, TGOSPA is evaluated using the LP metric [14]. The set of ground truth trajectories \mathbf{X} includes only *gt2* and *gt6* for the 61 frames considered (the final time step is $K=60$). The TGOSPA parameters are chosen to elucidate, especially the effect of the switching penalty γ , and show how it can be used for different purposes. In particular, the following four key configurations are used and presented in each of the following tables.

- **Gamma zero:** $\gamma=0$ and no switches are assessed. This case can be implemented using the simpler GOSPA metric at each time step and can be used for applications where information concerning trajectories is not present or needed, such as for training visual object detectors. Recall that TGOSPA with such a choice is not a metric on the space of finite sets of trajectories.
- **Gamma small:** $\gamma \in (0, \frac{c}{\sqrt[3]{2}})$ is selected according to the method proposed in Section 1 to detect and penalize short-term track changes. The particular value of γ (18) has been selected such that the threshold distance $g_1 = \frac{3}{4}c$ regardless of p . The interpretation of g_1 is given in Fig. 7. Such parametrization could be used for applications where any track change matters, such as for assessing and training re-ID modules.
- **Gamma large:** $\gamma = n^{1/p}c$ with $n=10$ is selected according to the method proposed in Section 2 to detect and penalize long-term track changes lasting for at least 11 time steps. Such parametrization could be used for most practical tracking applications to conveniently assess track changes such as illustrated in Fig. 8, or to assess how tracking algorithms cope with occlusions such as illustrated in Fig. 9.
- **Gamma extreme:** $\gamma = n^{1/p}c$ with $n=31 > \frac{K+1}{2} = 30.5$ is selected according to the findings of Section 2 to neglect *any* switches that may arise in the studied scenario consisting of 61 frames. As trajectories are assigned one-to-one, track changes that may be recognized as switches by humans are treated as pairs of

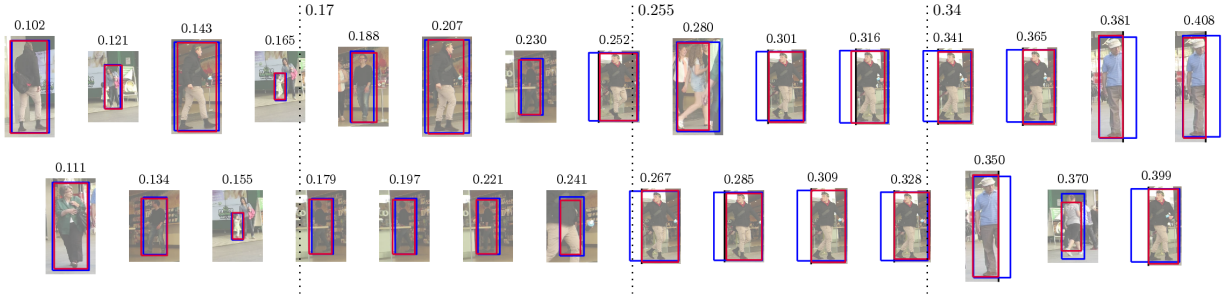


Fig. 12: Examples of bounding box pairs ordered using the IoU-induced metric. The value of the metric is given above each pair of boxes such that it grows from left to right. Each blue box is a ground truth box, while each red one is an estimate. The examples are drawn based on Fig. 11.

missed and false targets within the evaluation. This case can be implemented in a simplified manner [15, Sec. IV.C].

The remaining TGOSPA metric parameters were chosen based on Figures 11 and 12. The evaluation results are given in Tables II, III, and IV where the following three combinations of the parameters p and c are used:

- **Combination A:** the cut-off $c=0.34$ is chosen as the right endpoint of Interval I_2 and $p=1$ so that $a=\frac{c}{\sqrt{2}}=0.17$ is the left endpoint of I_2 .
- **Combination B:** the cut-off $c=0.255$ is chosen as the middle point of Interval I_2 and $p=1.71$ so that $a=0.17$ is the left endpoint of I_2 as before.
- **Combination C:** the cut-off $c=0.34$ is chosen as the right endpoint of Interval I_2 and $p=2.409$ so that $a=0.255$ is the middle endpoint of I_2 .

The IoU-induced metric d_{IoU} for bounding boxes was used in all the examples. Every cell of each table II, III and IV shows the value of the metric and its decomposition as shown in Fig. 14. For a given algorithm results contained in \mathbf{Y} and $\pi_*^{0:K}$ resulting from solving (5) (or (13)), the value

$$\bar{d}_p(\mathbf{X}, \mathbf{Y}, \pi_*^{0:K}) = \left(\frac{L_p^{(c)}(\mathbf{X}, \mathbf{Y}, \pi_*^{0:K})}{N^{(c)}(\mathbf{X}, \mathbf{Y}, \pi_*^{0:K})} \right)^{1/p}, \quad (34)$$

is the p -average localization error.

To visualize the data, distances between the estimates and ground truth bounding boxes are shown in Fig. 13. It should be noted that the studied data do not contain any *distant* false alarms or estimates that might be associated when increasing the value of c beyond 0.34. It can be seen that most estimates have errors lower than 0.17 in the IoU-induced metric (except for BoT_SORT at the 16-th time step), and there are significant errors merely during the occlusion of *gt6* either due to missing estimates (FRCNN, Tractor++v2) or slightly more distant estimates (BoT_SORT, GMPHDOG17). For the track fragmentation appearing in Tractor++v2, the length of the corresponding track change is $\ell=22$ as defined in Section 2 (i.e., assuming its first estimated trajectory is assigned to *gt6*).

Next, several observations are pointed out based on the results from Fig. 13, and Tables II, III, and IV.

A. Observations and Discussion

Observation 1 (track changes are found): Whenever using **Gamma zero**, no track changes are assessed. Using **Gamma small**, both short-term interim and long-term track changes are found and penalized for. That is, short-term interim track changes cannot be found without counting long-term ones at the same time. With increasing γ further to **Gamma large**, only long-term track changes are found and penalized. Using **Gamma extreme**, no switches arise, and all the track changes are assessed as missed and false estimates, which can be seen in the TGOSPA decomposition.

Observation 2 (algorithm with no track changes): The GMPHDOG17 tracker has no track changes, and the value of TGOSPA is thus independent of the choice of γ among all Tables II, III and IV. The TGOSPA values for the other algorithms thus increase with increasing γ .

Observation 3 (detector evaluation is meaningful only with $\gamma=0$): As FRCNN outputs are temporarily disconnected, switches arise when **Gamma small** is used. Increasing γ further makes any switches too costly, and all (but the closest estimate to each ground truth trajectory) are treated as false estimates. Thus, for detector training, only **Gamma zero** is recommended.

Observation 4 (TGOSPA metric is non-decreasing with increasing value of γ): Values in each row in Tables II, III and IV increase (or stay the same) from left to right.

That is, although no switches are counted in the decomposition for **Gamma extreme** on the one hand, the corresponding TGOSPA metric values are largest among the different γ setups. It can be seen that track changes that are present in the data are penalized using **Gamma extreme** with the maximum possible yield (the longer the track change, the higher the value), but TGOSPA does *not* show this fact in the decomposition which is undesirable for understanding the results and making further decisions.

Observing that both **Gamma large** and **Gamma extreme** setups lead to the same *ordering* of the algorithms (regardless of the parameters p and c), one can use **Gamma large** instead of **Gamma extreme** and observe

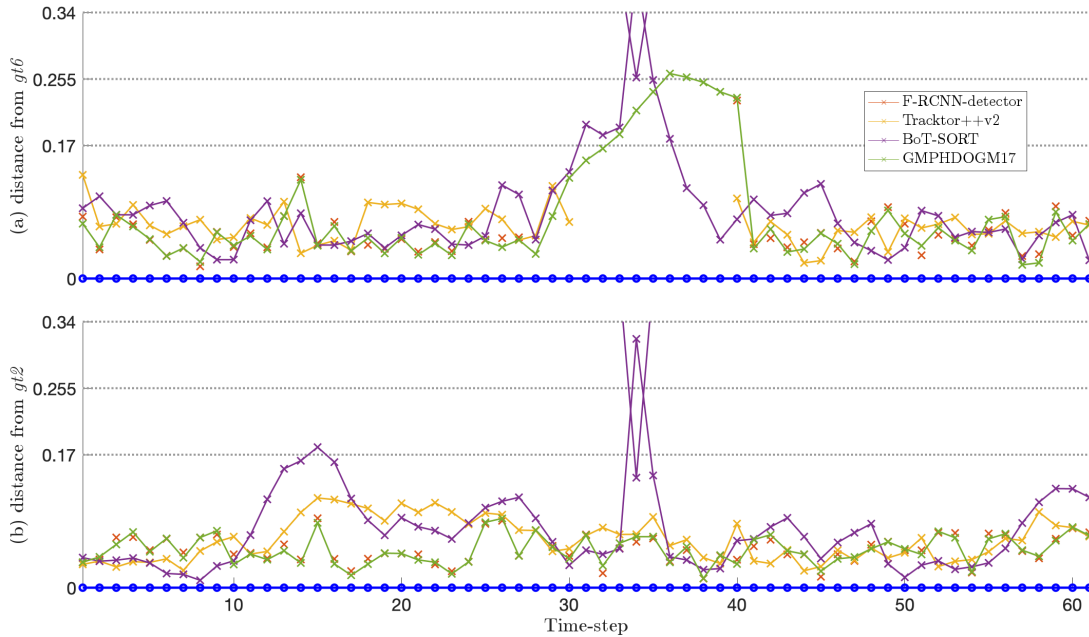


Fig. 13: The IoU-induced distance of individual estimates from each ground truth bounding box. Note that the F-RCNN detections depicted in red are not connected in time, and each detection is treated as a single trajectory containing a single object instance. There are two different trajectories for Tractor++v2 in Subfigure (a), depicted in yellow.

the decomposition such that the found switches correspond to track change with minimal length of $\ell=n+1=11$. Considering the meaning of the track change length and thus the kind of track change that are penalized (Section 2), the use of **Gamma extreme** in practice is not recommended.

Observation 5 (algorithm ordering based on the type of track change): The lengths of track changes clearly matter, which can be seen for BoT_SORT and Tractor++v2 in **Combination A** and **Combination B**: BoT_SORT is worse than Tractor++v2 using **Gamma small**, but it is better for **Gamma large**. On the other hand, according to Table IV for **Combination C**, the algorithms are given the same ordering regardless of γ . The ordering thus does not necessarily reflect the number of switches or their length, as the final TGOSPA metric value considers all the different error types jointly based on the chosen parameters. It can be seen from the corresponding decomposition that the switches found in BoT_SORT have little effect on the final value of the metric for **Gamma small** using **Combination C**, which is mainly due to the large value of $p=2.409$ selected.

Observation 6 (increasing p): From Table IV, the impact of localization error is mitigated with the large p in favor of the missed/false cost. Furthermore, switches can have even larger impact on the final TGOSPA metric value depending on the relative value of γ compared to c : for $\gamma > \frac{c}{\sqrt[p]{p}}$ (e.g., for **Gamma large**), even small number of switches has considerably larger impact to the final TGOSPA metric value compared to missed/false estimates and vice versa.

Observation 7 (the effect of non-admissible estimates): Consider the FRCNN detector and the GMPHDOG17 tracker in Tables II and IV for **Combination A** and **Combination C**, respectively, with **Gamma zero**. From Fig. 13, it follows that while the pedestrian *gt6* is visible (not occluded), estimates from both FRCNN and GMPHDOG17 algorithms have both errors lower than 0.17 in the IoU-induced metric. During the occlusion of *gt6*, estimates are missing for the FRCNN detector, while most estimates of the GMPHDOG17 tracker have errors larger than 0.17. In Table II, the TGOSPA metric values with **Gamma zero** for the two algorithms are nearly the same: the 12 missed objects of the FRCNN detector are slightly better than the non-admissible (larger than $a=0.17$) estimates appearing in the GMPHDOG17 tracker. In Table IV, however, the fine localization of the FRCNN detector evaluated with **Gamma zero** has a negligible effect (0.133) compared to the missed detection cost (0.446) corresponding to 12 missed estimates, which is the effect of large p .

Observation 8 (the effect of smaller c): Although p in **Combination B** has increased relative to **Combination A**, it can be seen that the cost of missed/false estimate $\frac{c^p}{2} \approx 0.048$ has decreased, and thus the localization error plays a dominant role especially for **Gamma zero**. Note that $c=0.255$ cuts off two estimates in the GMPHDOG17 and one from BoT_SORT that are treated as false estimates.

Observation 9 (two short-term interim track changes resulting into three switches only): For **Combination B** using **Gamma small**, BoT_SORT is found to have only

three switches instead of the expected four switches for the *two* short-term interim track changes (see Section 1). This is due to the estimate with error larger than $c=0.255$ at the 34-th time step being cut off: denoting with index 1 the corresponding BoT_SORT trajectory that tracks $gt2$, the resulting assignment for $gt6$ is $[\dots, 1, 0, 1, \dots] = [\pi_{\star}^{\dots 33, 34, 35, \dots}]_{i="gt6"}$, which leads to two subsequent half-switches.

Observation 10 (BoT_SORT estimate is larger than $g_1=0.255$ but results into switches anyway): For **Combination A** using **Gamma small**, the BoT_SORT estimate discussed above is larger than g_1 , and a total of four switches were found. The reason is that the assumptions introduced in Section 1 do not apply in this particular case since the value of c is larger (the distance from $gt2$ to the estimate is smaller than c , i.e., $d(x_{gt2}^{34}, y_1^{34}) < c$). It turns out that the threshold (for the distance so that a switch results) for such a case is smaller than $g_1=0.255$.

Note that for algorithms yielding similar TGOSPA metric values, decomposition can be used to explain the efficiency of the algorithms. In particular, the TGOSPA metric decomposition can be easily defined over time offering further insight into the algorithm's behavior. This is not the case for the HOTA score that uses averaging over different threshold values. Note that the TGOSPA metric and HOTA score are further compared in the next Section.

VII. HOTA vs. TGOSPA

In this section, we prove that HOTA (defined in Appendix) does not satisfy the triangle inequality. TGOSPA and HOTA are then compared using five toy examples, illustrated in Fig. 15.

As discussed before, HOTA is not a metric on the space of sets of trajectories $\mathcal{F}(\mathcal{T}(\mathcal{X}))$ and may have undesirable properties, which is illustrated in the following.

Proposition 1 (HOTA does not satisfy the triangle inequality): Consider three sets of trajectories $\mathbf{X}=\{X_1\}$, $\mathbf{Y}=\{X_1\}$ and $\mathbf{Z}=\emptyset$, where X_1 is an arbitrary trajectory. In this case, we obtain $\text{HOTA}(\mathbf{X}, \mathbf{Y})=1$, $\text{HOTA}(\mathbf{X}, \mathbf{Z})=0$, and $\text{HOTA}(\mathbf{Y}, \mathbf{Z})=0$. As a result,

$$\text{HOTA}(\mathbf{X}, \mathbf{Y}) \not\leq \text{HOTA}(\mathbf{X}, \mathbf{Z}) + \text{HOTA}(\mathbf{Z}, \mathbf{Y}), \quad (35)$$

which means that HOTA does not satisfy the triangle inequality that is required of (mathematical) metrics. \square

A. Toy Examples Comparing TGOSPA and HOTA

The following five examples, Ex1-Ex5, are depicted in Fig. 15a-15e, and the corresponding ranking is summarized in Table V. Note that perfect localization is considered in the toy examples, so the threshold parameter α in HOTA plays no role. Furthermore, c is assumed *small* for the TGOSPA metric so that the outlying estimates Ex2, Ex3, and Ex5 result in false alarms. In addition,

two choices of γ for the TGOSPA metric are used so that the track changes in Fig. 15a either are considered as switches in the metric (which is desirable for the perfect localization) or not, respectively.

1. Ex1: Perfect localization and two track switches

The TGOSPA metric with $\gamma < c$ is $d_p^{(c, \gamma)}(\mathbf{X}, \mathbf{Y})=2\gamma$ and two switches are found. For $\gamma > c$, however, it is $d_p^{(c, \gamma)}(\mathbf{X}, \mathbf{Y})=4 \times \frac{c}{2}=2c$ and two pairs of missed and false estimates result. The HOTA score for Ex1 is

$$\text{HOTA}(\mathbf{X}, \mathbf{Y}) = \sqrt{\frac{4 \times \frac{1}{1+1+1}}{2+1+1}} \approx 0.577. \quad (36)$$

2. Ex2: Perfect Localization, One Missed, and One False

For this and the following Ex3, Ex4 and Ex5, the TGOSPA metric is independent of the choice of γ . In this case, TGOSPA: $d_p^{(c, \gamma)}(\mathbf{X}, \mathbf{Y})=2 \times \frac{c}{2}=c$, whereas

$$\text{HOTA}(\mathbf{X}, \mathbf{Y}) = \sqrt{\frac{\frac{1}{1+0+0} + \frac{1}{1+0+0} + \frac{1}{1+1+1}}{3+1+1}} \approx 0.683. \quad (37)$$

3. Ex3: Perfect Localization, Two Missed, and Two False

TGOSPA: $d_p^{(c, \gamma)}(\mathbf{X}, \mathbf{Y})=4 \times \frac{c}{2}=2c$, whereas

$$\text{HOTA}(\mathbf{X}, \mathbf{Y}) = \sqrt{\frac{\frac{1}{1+0+0} + \frac{1}{1+0+0}}{2+2+2}} \approx 0.577. \quad (38)$$

4. Ex4: All Missed

TGOSPA: $d_p^{(c, \gamma)}(\mathbf{X}, \mathbf{Y})=4 \times \frac{c}{2}=2c$, whereas $\text{HOTA}=0$.

5. Ex5: All Missed and Two False

TGOSPA: $d_p^{(c, \gamma)}(\mathbf{X}, \mathbf{Y})=6 \times \frac{c}{2}=3c$, whereas $\text{HOTA}=0$.

From the HOTA scores in different examples, we can observe that the considered tracker:

- 1) has the same performance in Ex1 and Ex3.
- 2) has the best performance in Ex2.
- 3) has the worst performance in Ex4 and Ex5.

The ranking of tracking performance based on HOTA in these examples may not always be desirable for different applications. It makes sense that the case with two missed and two false estimates (Ex3) is worse than the case with only one missed and one false estimate (Ex2). However, *should the case with two track changes (Ex1) be worse than the case with only one missed and one false detection (Ex3)?* This should be application dependent, and for this to be possible, hyper-parameters should be introduced such that missed detection, false detection, and track switches can be penalized differently. This is employed in the TGOSPA metric to some level²²: for small $\gamma < c$ Ex1 is better than Ex3 and for large $\gamma > c$, Ex1 performs the same as Ex3. Moreover, we can observe that HOTA yields unintuitive results in Ex4 and Ex5, as it does not penalize the additional false detections in Ex5.

²²Remind that missed and false object instances are both penalized with the same value $\frac{c^p}{2}$ in TGOSPA.

TABLE II: **Combination A**: valuation using the IoU metric with TGOSPA parameters $p=1$ and $c=0.34$ ($a=0.17$).

	Gamma zero No switch matter $\gamma = 0$ (GOSPA)			Gamma small Any switch matter (the more, the worse) $\gamma = 0.043$ $g_1 = 0.255$			Gamma large Only switches lasting for $\ell > 10$ time steps matter $\gamma = 3.4, (n = 10)$ $h_{10} = 0, h_{11} = 0.0309$			Gamma extreme One-to-one trajectory matching “ $\gamma \rightarrow \infty$ ” $h_\ell = 0, \forall \ell \leq \frac{\text{no. frames}}{2}$		
	FRCNN <i>temporarily disconnected estimates</i>	0.053 7.828	5.788 2.04	110 12	0.053 12.418	5.788 2.04	110 12	0.014 38.787	0.027 20.4	2 120	0.014 38.787	0.027 20.4
Tracktor++v2 <i>1×long-term track change</i>	0.064 8.791	7.261 1.53	113 9	0.064 8.833	7.261 1.53	113 9	0.064 12.191	7.261 3.4	113 9	0.065 14.929	5.919 5.27	91 31
BoT_SORT <i>2×short-term interim track change</i>	0.076 9.28	9.28 0	122 0	0.076 9.45	9.28 0.17	122 4	0.076 9.541	9.201 0.17	121 1	0.076 9.541	9.201 0.17	121 1
GMPHDOGM17 <i>no track change</i>	0.064 7.867	7.867 0	122 0	0.064 7.867	7.867 0	122 0	0.064 7.867	7.867 0	122 0	0.064 7.867	7.867 0	122 0

 TABLE III: **Combination B**: valuation using the IoU metric with TGOSPA parameters $p=1.71$ and $c=0.255$ ($a=0.17$).

	Gamma zero No switch matter $\gamma = 0$ (GOSPA)			Gamma small Any switch matter (the more, the worse) $\gamma = 0.079$ $g_1 = 0.2125$			Gamma large Only switches lasting for $\ell > 10$ time steps matter $\gamma = 0.981, (n = 10)$ $h_{10} = 0, h_{11} = 0.0627$			Gamma extreme One-to-one trajectory matching “ $\gamma \rightarrow \infty$ ” $h_\ell = 0, \forall \ell \leq \frac{\text{no. frames}}{2}$		
	FRCNN <i>temporarily disconnected estimates</i>	0.057 1.213	0.811 0.58	110 12	0.057 1.822	0.811 1.398	110 12	0.014 4.072	0.001 5.803	2 120	0.014 4.072	0.001 5.803
Tracktor++v2 <i>1×long-term track change</i>	0.068 1.299	1.128 0.435	113 9	0.068 1.305	1.128 0.013	113 9	0.068 1.721	1.128 0.967	113 9	0.069 2.08	0.933 1.499	91 31
BoT_SORT <i>2×short-term interim track change</i>	0.083 1.423	1.73 0.048	121 1	0.083 1.44	1.73 0.039	121 3	0.083 1.45	1.695 0	120 0	0.083 1.45	1.695 0	120 0
GMPHDOGM17 <i>no track change</i>	0.071 1.271	1.314 0.097	120 2	0.071 1.271	1.314 0.097	120 2	0.071 1.271	1.314 0.097	120 2	0.071 1.271	1.314 0.097	120 2

 TABLE IV: **Combination C**: valuation using the IoU metric with TGOSPA parameters $p=2.409$ and $c=0.34$ ($a=0.255$).

	Gamma zero No switch matter $\gamma = 0$ (GOSPA)			Gamma small Any switch matter (the more, the worse) $\gamma = 0.149$ $g_1 = 0.2975$			Gamma large Only switches lasting for $\ell > 10$ time steps matter $\gamma = 0.884, (n = 10)$ $h_{10} = 0, h_{11} = 0.1257$			Gamma extreme One-to-one trajectory matching “ $\gamma \rightarrow \infty$ ” $h_\ell = 0, \forall \ell \leq \frac{\text{no. frames}}{2}$		
	FRCNN <i>temporarily disconnected estimates</i>	0.062 0.797	0.133 0.446	110 12	0.062 1.241	0.133 1.104	110 12	0.014 2.428	0.000 4.46	2 120	0.014 2.428	0.000 4.46
Tracktor++v2 <i>1×long-term track change</i>	0.071 0.765	0.19 0.334	113 9	0.071 0.771	0.19 0.01	113 9	0.071 1.103	0.19 0.743	113 9	0.072 1.369	0.16 1.152	91 31
BoT_SORT <i>2×short-term interim track change</i>	0.095 0.699	0.422 0	122 0	0.095 0.726	0.422 0.041	122 4	0.097 0.758	0.439 0	121 1	0.097 0.758	0.439 0	121 1
GMPHDOGM17 <i>no track change</i>	0.091 0.67	0.381 0	122 0	0.091 0.67	0.381 0	122 0	0.091 0.67	0.381 0	122 0	0.091 0.67	0.381 0	122 0

that properly track the particular ground truth trajectory i among the time steps. The set $\mathcal{M}_A(k, i, j, \mathbf{X}, \pi^{0:K})$ contains links to ground truth objects out of the trajectory i that *are not* properly tracked by the particular estimated trajectory j among the time steps. Furthermore, the set $\mathcal{F}_A(k, i, j, \mathbf{Y}, \pi^{0:K})$ contains links to estimates out of the trajectory j that *do not* properly track the particular ground truth trajectory i among the time steps. An illustration of the above-defined sets is given in Fig. 16.

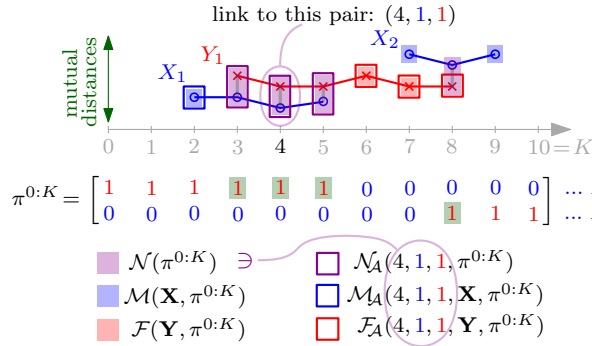


Fig. 16: Illustration of sets involved in the HOTA score computation. The sets on the left concern all trajectories, but the sets on the right regard only the two trajectories to which the input link (k, i, j) belongs.

With this notation, according to [10], the HOTA score is defined as follows.

Definition 2 (HOTA score): Given two trajectories \mathbf{X} and \mathbf{Y} , the HOTA score is defined and approximated as

$$\text{HOTA}(\mathbf{X}, \mathbf{Y}) = \int_0^1 \text{HOTA}^{(\alpha)}(\mathbf{X}, \mathbf{Y}) d\alpha \quad (45a)$$

$$\approx \frac{1}{19} \sum_{l=1}^{19} \text{HOTA}^{(0.05 \cdot l)}(\mathbf{X}, \mathbf{Y}), \quad (45b)$$

where HOTA for the *threshold*²⁴ $\alpha > 0$ is defined as

$$\text{HOTA}^{(\alpha)}(\mathbf{X}, \mathbf{Y}) = \frac{\sum_{(k,i,j) \in \mathcal{N}(\pi_{*,\alpha}^{0:K})} \mathcal{A}_{\mathbf{X},\mathbf{Y}}(k, i, j, \pi_{*,\alpha}^{0:K})}{\sqrt{|\mathcal{N}(\pi_{*,\alpha}^{0:K})| + |\mathcal{M}(\mathbf{X}, \pi_{*,\alpha}^{0:K})| + |\mathcal{F}(\mathbf{Y}, \pi_{*,\alpha}^{0:K})|}}, \quad (46)$$

where $\mathcal{A}_{\mathbf{X},\mathbf{Y}}(k, i, j, \pi_{*,\alpha}^{0:K})$ is the *assignment score*

$$\mathcal{A}_{\mathbf{X},\mathbf{Y}}(k, i, j, \pi_{*,\alpha}^{0:K}) = \frac{|\mathcal{N}_A(k, i, j, \pi_{*,\alpha}^{0:K})|}{|\mathcal{N}_A(k, i, j, \pi_{*,\alpha}^{0:K})| + |\mathcal{M}_A(k, i, j, \mathbf{X}, \pi_{*,\alpha}^{0:K})| + |\mathcal{F}_A(k, i, j, \mathbf{Y}, \pi_{*,\alpha}^{0:K})|}. \quad (47)$$

The assignments $\pi_{*,\alpha}^{0:K} = [\pi_{*,\alpha}^0(\alpha), \dots, \pi_{*,\alpha}^K(\alpha)]$ are computed individually for each time step (using the Hungarian algorithm), which can be written as

$$\pi_{*,\alpha}^k(\alpha) = \arg \min_{\pi^k} \sum_{(i,j) \in \rho(\pi^k)} \text{MS}^{(\alpha)}(\mathbf{x}_i^k, \mathbf{y}_j^k, \pi^k) \quad (48)$$

where $\text{MS}^{(\alpha)}(\mathbf{x}_i^k, \mathbf{y}_j^k, \pi^k)$ is the *scoring function for potential matches* defined as

$$\text{MS}^{(\alpha)}(\mathbf{x}_i^k, \mathbf{y}_j^k, \pi^k) = \frac{1}{\epsilon} + \mathcal{A}_{\max}^{(\alpha)}(i, j) + \epsilon \cdot \mathcal{S}(x_i^k, y_j^k), \quad (49)$$

²⁴Notice that the threshold parameter α is analogous to the cut-off parameter in TGOSPA with $c=1-\alpha$.

if $(\mathbf{x}_i^k = \{x_i^k\}, \mathbf{y}_j^k = \{y_j^k\})$ and $\mathcal{S}(x_i^k, y_j^k) > \alpha$ and zero otherwise; the number ϵ is a "small number such that the components have different magnitudes," and \mathcal{S} is a chosen *similarity score* for object instances such as the IoU (27) for bounding boxes. The function $\mathcal{A}_{\max}^{(\alpha)}(i, j)$ is the maximum assignment score possible for the particular pair (k, i, j) , which is equal to

$$\mathcal{A}_{\max}^{(\alpha)}(i, j) = \mathcal{A}_{\mathbf{X},\mathbf{Y}}(k, i, j, \mu_{(i,j)}^{0:K}(\alpha)), \quad (50)$$

where the assignment $\mu_{(i,j)}^{0:K}(\alpha)$ is designed to assign trajectories i and j for all time steps wherever they both exist, and their similarity score is higher than α , i.e., it can be defined as a matrix of zeros and j 's (in the i -th row) as

$$[\mu_{(i,j)}^{0:K}(\alpha)]_{(k,i')} = \begin{cases} j & \text{if } i = i', \mathbf{x}_i^k = \{x_i^k\}, \mathbf{y}_j^k = \{y_j^k\} \\ & \text{and } \mathcal{S}(x_i^k, y_j^k) > \alpha, \\ 0 & \text{otherwise.} \end{cases} \quad (51)$$

where $[\cdot]_{(k',i')}$ is the (k', i') -th element of the input matrix. \square

From Fig. 16, notice that the so-called assignment score $\mathcal{A}_{\mathbf{X},\mathbf{Y}}(k, i, j, \pi_{*,\alpha}^{0:K})$ (47) can be understood as an *intersection over union* between the two trajectories to which the given link (k, i, j) "belongs".

REFERENCES

- [1] S. Blackman and R. Popoli, *Design and Analysis of Modern Tracking Systems*. Artech House, 1999.
- [2] Y. Bar-Shalom, P. K. Willet, and X. Tian, *Tracking and Data Fusion: A Handbook of Algorithms*. YBS Publishing, 2011.
- [3] B.-N. Vo, M. Mallick, Y. Bar-Shalom, S. Coraluppi, R. Osborne III, R. Mahler, and B.-T. Vo, *Multitarget Tracking*. Wiley Enc. of Electrical and Electronics Eng., 2015, pp. 1–15. [Online]. Available: <https://onlinelibrary.wiley.com/doi/abs/10.1002/047134608X.W8275>
- [4] Á. F. García-Fernández, L. Svensson, and M. R. Morelande, "Multiple target tracking based on sets of trajectories," *Accepted for the IEEE Trans. on Aerospace and Electronic Systems*, 2019.
- [5] J. Krejčí, O. Straka, J. Vyskočil, M. Jiřík, and U. Dahmen, "Feature-based multi-object tracking with maximally one object per class," in *2022 25th International Conference on Information Fusion (FUSION)*, 2022, pp. 1–8.
- [6] W. Faber, S. Chakravorty, and I. I. Hussein, "Multi-object tracking with multiple birth, death, and spawn scenarios using a randomized hypothesis generation technique (rfisst)," in *2016 19th Int. Conf. on Inf. Fus. (FUSION)*, 2016, pp. 154–161.
- [7] S. Coraluppi, "Advances in multi-target tracking performance evaluation," in *2023 26th International Conference on Information Fusion (FUSION)*, 2023, pp. 1–7.
- [8] K. Bernardin and R. Stiefelhagen, "Evaluating multiple object tracking performance: The clear mot metrics," *EURASIP Journal on Image and Video Processing*, vol. 2008, no. 1, p. 246309, 2008. [Online]. Available: <https://doi.org/10.1155/2008/246309>
- [9] A. Milan, L. Leal-Taixe, I. Reid, S. Roth, and K. Schindler, "MOT16: A benchmark for multi-object tracking," *arXiv:1603.00831*, 2016.
- [10] J. Luiten, A. Ošep, P. Dendorfer, P. Torr, A. Geiger, L. Leal-Taixé, and B. Leibe, "HOTA: A higher order metric for evaluating multi-object tracking," *International Journal of Computer Vision*, vol. 129, no. 2, pp. 548–578, 2021. [Online]. Available: <https://doi.org/10.1007/s11263-020-01375-2>

- [11] G. Brasó and L. Leal-Taixé, "Learning a neural solver for multiple object tracking," in *2020 IEEE/CVF Conference on Computer Vision and Pattern Recognition (CVPR)*, 2020, pp. 6246–6256.
- [12] A. Milan, L. Leal-Taixé, I. Reid, S. Roth, and K. Schindler, "website of Multiple Object Tracking Benchmark MOT17," at <https://motchallenge.net/data/MOT17/>, last checked 2024 Nov. 1.
- [13] T. M. Apostol, *Mathematical Analysis*. Addison Wesley, 1974.
- [14] Á. F. García-Fernández, A. S. Rahmathullah, and L. Svensson, "A metric on the space of finite sets of trajectories for evaluation of multi-target tracking algorithms," *IEEE Transactions on Signal Processing*, vol. 68, pp. 3917–3928, 2020.
- [15] —, "A time-weighted metric for sets of trajectories to assess multi-object tracking algorithms," in *2021 IEEE 24th International Conference on Information Fusion (FUSION)*, 2021, pp. 1–8.
- [16] J. Bento and J. J. Zhu, "A metric for sets of trajectories that is practical and mathematically consistent," 2020. [Online]. Available: <https://arxiv.org/abs/1601.03094>
- [17] M. Beard, B. T. Vo, and B.-N. Vo, "A solution for large-scale multi-object tracking," *IEEE Transactions on Signal Processing*, vol. 68, pp. 2754–2769, 2020.
- [18] B. Ristic, B.-N. Vo, D. Clark, and B.-T. Vo, "A metric for performance evaluation of multi-target tracking algorithms," *IEEE Trans. on Signal Processing*, vol. 59, no. 7, pp. 3452–3457, 2011.
- [19] T. Vu and R. Evans, "A new performance metric for multiple target tracking based on optimal subpattern assignment," in *17th Int. Conf. on Information Fusion (FUSION)*, 2014, pp. 1–8.
- [20] K. Simonyan and A. Zisserman, "Very deep convolutional networks for large-scale image recognition," in *3rd International Conference on Learning Representations, ICLR 2015, San Diego, CA, USA, May 7-9, 2015, Conference Track Proceedings*, Y. Bengio and Y. LeCun, Eds., 2015. [Online]. Available: <http://arxiv.org/abs/1409.1556>
- [21] P. Bergmann, T. Meinhardt, and L. Leal-Taixé, "Tracking without bells and whistles," in *2019 IEEE/CVF International Conference on Computer Vision (ICCV)*. Los Alamitos, CA, USA: IEEE Computer Society, nov 2019, pp. 941–951. [Online]. Available: <https://doi.ieeecomputersociety.org/10.1109/ICCV.2019.00103>
- [22] N. Aharon, R. Orfaig, and B.-Z. Bobrovsky, "BoT-SORT: Robust associations multi-pedestrian tracking," arXiv:2206.14651, 2022. [Online]. Available: <https://arxiv.org/abs/2206.14651>
- [23] Z. Ge, S. Liu, F. Wang, Z. Li, and J. Sun, "Yolox: Exceeding yolo series in 2021," 2021. [Online]. Available: <https://arxiv.org/abs/2107.08430>
- [24] Y.-M. Song, K. Yoon, Y.-C. Yoon, K. C. Yow, and M. Jeon, "Online multi-object tracking with gmphd filter and occlusion group management," *IEEE Access*, vol. 7, pp. 165 103–165 121, 2019.
- [25] B.-N. Vo, S. Singh, and A. Doucet, "Sequential monte carlo methods for multitarget filtering with random finite sets," *IEEE Transactions on Aerospace and Electronic Systems*, vol. 41, no. 4, pp. 1224–1245, 2005.
- [26] J. Krejčí, O. Kost, and O. Straka, "Bounding box detection in visual tracking: Measurement model parameter estimation," in *2023 26th Int. Conf. on Inf. Fus. (FUSION)*, 2023, pp. 1–8.
- [27] A. S. Rahmathullah, Á. F. García-Fernández, and L. Svensson, "Generalized optimal sub-pattern assignment metric," in *2017 20th Int. Conf. on Inf. Fus. (Fusion)*, 2017, pp. 1–8.
- [28] V. Nevelius Wernholm and A. Wärnsäter, "Efficient evaluation of target tracking using entropic optimal transport," Master's thesis, Chalmers University of Technology, 2024.
- [29] I. Goodman, H. T. Nguyen, and R. Mahler, *Mathematics of Data Fusion*. Kluwer Academic Publishers, 1997.
- [30] D. Stoyan, W. S. Kendall, and J. Mecke, *Stochastic Geometry and its Applications, 2nd edition*. Wiley, September 1995.
- [31] M. Chavent, "A hausdorff distance between hyper-rectangles for clustering interval data," in *Classification, Clustering, and Data Mining Applications*, D. Banks, F. R. McMorris, P. Arabia, and W. Gaul, Eds. Springer Berlin Heidelberg, 2004, pp. 333–339.
- [32] C. Villani, *Topics in Optimal Transportation*. American Mathematical Society, 2003, vol. 58.
- [33] A. Iripino and R. Verde, "Dynamic clustering of interval data using a wasserstein-based distance," *Pattern Recognition Letters*, vol. 29, no. 11, pp. 1648–1658, 2008. [Online]. Available: <https://www.sciencedirect.com/science/article/pii/S0167865508001396>
- [34] H. Rezatofighi, N. Tsoi, J. Gwak, A. Sadeghian, I. Reid, and S. Savarese, "Generalized intersection over union," in *The IEEE Conf. on Computer Vision and Pat. Rec. (CVPR)*, June 2019.
- [35] B. Cheng, R. Girshick, P. Dollar, A. C. Berg, and A. Kirillov, "Boundary iou: Improving object-centric image segmentation evaluation," in *Proceedings of the IEEE/CVF Conf. on Computer Vision and Pat. Rec. (CVPR)*, June 2021, pp. 15 334–15 342.
- [36] Z. Zheng, P. Wang, D. Ren, W. Liu, R. Ye, Q. Hu, and W. Zuo, "Enhancing geometric factors in model learning and inference for object detection and instance segmentation," *IEEE Transactions on Cybernetics*, vol. 52, no. 8, pp. 8574–8586, 2022.
- [37] W. Rudin, *Real and Complex Analysis*, international ed. McGraw-Hill, New York, 1987.
- [38] M. Levandowsky and D. Winter, "Distance between sets," *Nature*, vol. 234, no. 5323, pp. 34–35, 1971. [Online]. Available: <https://doi.org/10.1038/234034a0>